14 Time-Resolved Energy Transfer and Conformational Distributions of Biopolymers

In the previous chapter we described the principles of resonance energy transfer (RET), and how the phenomenon could be used to measure distances between donor and acceptor sites on macromolecules or the association between donor-labeled and acceptor-labeled biomolecules. Energy transfer was described as a through-space interaction that occurred whenever the emission spectrum of the donor overlapped with the absorption spectrum of the acceptor. For a given donor–acceptor (D–A) pair, the efficiency of energy transfer decreases as r^{-6}, where r is the D–A distance. Each D–A pair has a characteristic distance: the Förster distance (R_0) at which RET is 50% efficient. The extent of energy transfer, as seen from the steady-state data, can be used to measure the distance, to study protein folding, to determine the extent of association based on proximity, or to create images of associated intracellular proteins.

In this chapter we describe more advanced applications of RET, particularly those that rely on time-resolved measurements of covalently linked D–A pairs. For such pairs the time-resolved data can be used to recover the conformational distribution or distance distribution between the donor and acceptor. Donor-to-acceptor motions also influence the extent of energy transfer, which can be used to recover the mutual diffusion coefficient. In Chapter 15 we will consider RET between donors and acceptors that are not covalently linked. In this case the extent of RET depends on the dimensional geometry of the molecules, such as planar distributions in membranes and one-dimensional distributions in double-helical DNA.

While the phenomenon of energy transfer is the same in all these situations, each application of RET requires a different theory to interpret the steady-state or time-resolved data. RET depends on the geometry and dynamics of the system, and thus provides a powerful yet complex methodology for studies of donor–acceptor distributions in any dimensionality.

14.1. DISTANCE DISTRIBUTIONS

In the previous chapter we considered energy transfer between a single donor (D) and acceptor (A) positioned at a unique distance (r). We now consider the case where a range of D–A distances is possible. This use of RET to study distance distributions was first reported by Haas, Steinberg, and coworkers using flexible polypeptides.[1–3] The concept of a distribution of donor-to-acceptor distances is shown in Figure 14.1. The protein is assumed to be labeled at unique sites by a single donor and single acceptor. In the native state one expects a single conformation and a single D–A distance. For the native state the distance is sharply localized at a particular value of r. This unique distance is expressed as a probability function $P(r)$ that is narrowly distributed along the r axis.

Now suppose the protein is unfolded to the random-coil state by the addition of denaturant. Since the peptide is in a random state, there exists a range of D–A distances. This range of conformations results in a range of accessible D–A distances, or a wide $P(r)$ distribution (Figure 14.1,

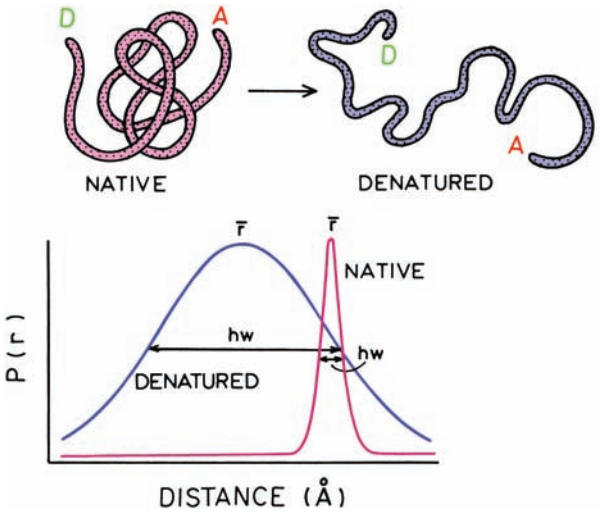

Figure 14.1. Distribution of D–A distance for a native and denatured protein. The probability functions $P(r)$ are peak normalized. In both cases the integrate probability should be unity.

lower panel). For visual clarity, the $P(r)$ distributions shown in Figure 14.1 are peak normalized, but the actual area under each curve should be normalized to unity to correspond to a single acceptor per donor.

The presence of a distribution of distances has a profound impact on the time-resolved decays of the donor. For the native protein the single D–A distance results in a single transfer rate for all the donors. Hence the decay time of the donor is shortened and is given by

$$I_{DA}(r,t) = I_D^0 \exp\left[-t/\tau_D - k_T(r)t\right] \qquad (14.1)$$

where τ_D is the decay time of the donor in the absence of acceptor, I_D^0 is the donor intensity at $t = 0$, and $k_T(r)$ is the D–A transfer rate, given by

$$k_T(r) = \frac{1}{\tau_D}\left(\frac{R_0}{r}\right)^6 \qquad (14.2)$$

Since there is only one distance and only one transfer rate $k_T(r) = k_T$, the donor decay remains a single exponential (Figure 14.2, top), and

$$I_{DA}(r,t) = I_{DA}(t) = I_D^0 \exp\left[-t/\tau_{DA}\right] \qquad (14.3)$$

where the lifetime in the presence of the acceptor, τ_{DA}, is given by

$$\frac{1}{\tau_{DA}} = \frac{1}{\tau_D} + k_T(r) \qquad (14.4)$$

It is this assumption of a single distance that allows calculation of the distance from the relative quantum yield of the donor (Chapter 13).

Now assume there is a range of D–A distances. For these simulated data we assumed a single-exponential

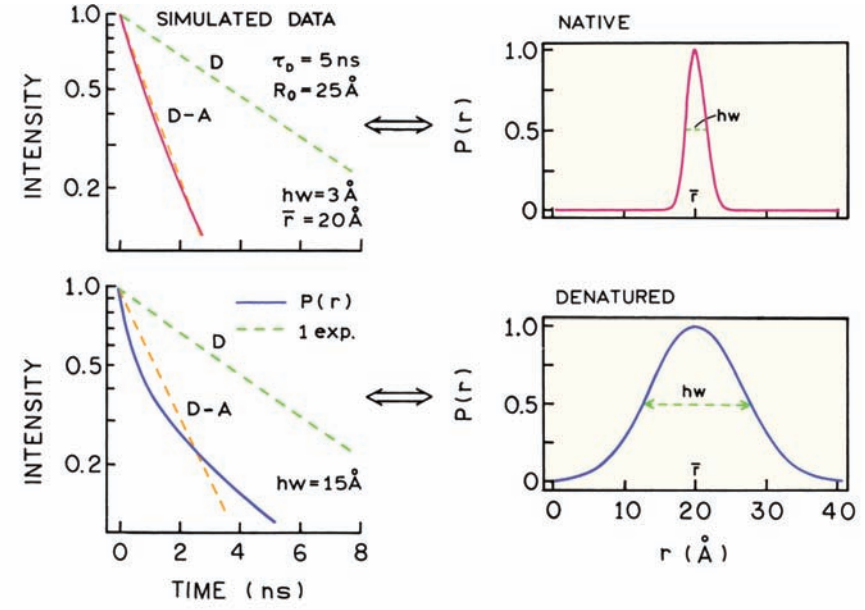

Figure 14.2. Effect of a distance distribution on the time-domain intensity decay of the donor.

decay time of 5 ns in the absence of acceptor, and R_0 = 25 Å. Some of the D–A pairs are closely spaced and display shorter decay times, and other D–A pairs are further apart and display longer decay times. The range of distances results in a range of decay times, so that the donor decay becomes more complex than a single exponential (Figure 14.2, bottom). Similar results are expected for frequency domain (FD) data. If there is a single D–A distance the frequency-domain intensity decay is well approximated by the single-exponential fit (Figure 14.3, top), which is shifted to higher frequencies by the presence of the acceptor. A range of D–A distances results in a frequency response that is spread out along the frequency axis, and one that is no longer a single exponential (Figure 14.3, bottom). The goal of most distance-distribution studies is to recover the D–A probability distribution from the non-exponential decays of the donor. This means that the shape of the intensity decays (Figure 14.2, left) are used to determine the D–A probability distribution (Figure 14.2, right). It is important to note the necessity of the time-resolved data to recover a distance distribution. For a distance distribution, measurement of the relative yield of the donor can be used to calculate an apparent distance, as was done in Problem 13.1. However, the steady-state data cannot be used to determine the distribution, and will not reveal the presence of a distribution. For the moment we have ignored donor-to-acceptor motions, which will be discussed in Section 14.7.

Irrespective of whether the donor intensity decays are measured in the time domain (TD) or frequency-domain (FD), the information content of the time-resolved data is limited. It is not practical to determine a distance distribution of arbitrary shape. For this reason it is common practice to describe the distribution using a limited number of parameters. The most appropriate and commonly used distribution is a Gaussian:

$$P(r) = \frac{1}{\sigma\sqrt{2\pi}} \exp\left[-\frac{1}{2}\left(\frac{\bar{r} - r}{\sigma}\right)^2 \right] \qquad (14.5)$$

In this equation $\bar{r}$ is the mean of the Gaussian with a standard deviation of σ. Usually distance distributions are described by the full width at half maxima (Figure 14.2, lower right). This half width (nm) is given by $hw = 2.354\sigma$. Distance distributions have also been expressed as Lorentzian[4] and other functions,[5–6] but the principles remain the same. With presently available data, distance distributions can be resolved, but it is difficult to distinguish the precise shape of the distribution.

What equation describes the intensity decay for a distance distribution? Unfortunately, the donor decay can only be described by an integral equation. The intensity decay for those D–A pairs at a distance r is given by eq. 14.1. Unless a single molecule is observed in a rigid medium, the D–A pairs with a unique distance r cannot be individually observed. Rather, one observes a weighted average determined by $P(r)$. The donor intensity decay is a summation of the intensity decays for all accessible distances, and is usually written as

$$I_{DA}(t) = \int_{r=0}^{\infty} P(r) I_{DA}(r,t)\, dr$$

$$= I_D^0 \int_{r=0}^{\infty} P(r) \exp\left[-\frac{t}{\tau_D} - \frac{t}{\tau_D}\left(\frac{R_0}{r}\right)^6 \right] dr \qquad (14.6)$$

This expression indicates that the intensity decay for an ensemble of flexible D–A pairs is given by the weighted average of the decays for each D–A distance.

Data analysis is performed by predicting the values of $I_{DA}(t)$ for use with time-domain or frequency-domain measurements and the usual procedures of nonlinear least squares. Typically the decay time of the donor (τ_D) is known from measurements of the donor in the absence of acceptor. The variable parameters in the analysis are those describing the distance distribution: $\bar{r}$ and hw.

This description of the intensity decay (eq. 14.6) illustrates the value of computer programs written in terms of the molecular features of the sample. The complex donor decays in the presence of acceptor (Figures 14.2 or 14.3) could be analyzed in terms of the multi-exponential model. While it would be possible to fit the data, the value of α_i and τ_i would only indirectly reflect the distance distribution. In contrast, programs based on eq. 14.6 provide direct information on $P(r)$.

14.2. DISTANCE DISTRIBUTIONS IN PEPTIDES

14.2.1. Comparison for a Rigid and Flexible Hexapeptide

The recover of distance distributions from the time-resolved (TD or FD) data is best understood by examining a specific example. Consider the two hexapeptides each containing a tryptophanamide ($TrpNH_2$) donor and a dansyl (DNS) acceptor (Figure 14.4).[7] One of the hexapeptides ($TrpNH_2$–$(pro)_6$–DNS) consists of six rigid prolyl residues that sepa-

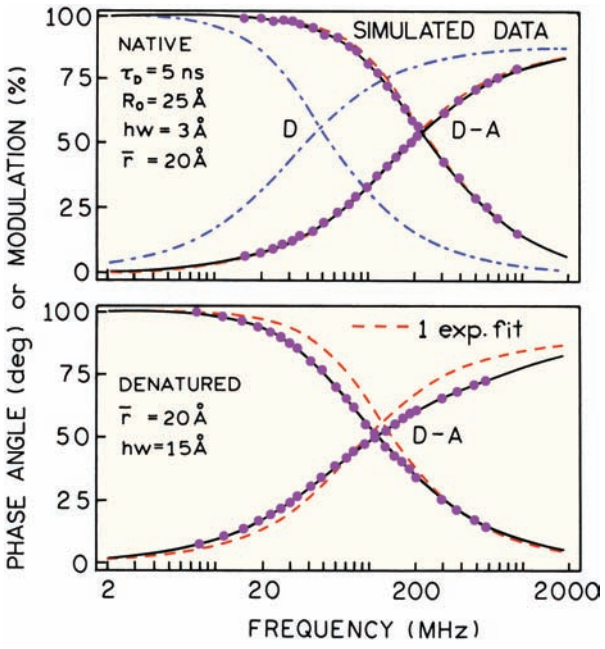

Figure 14.3. Effect of a distance distribution on the frequency-domain intensity decay of the donor. The dashed line shows the best single-exponential fit to the simulated data.

rate Trp and DNS by a single distance. The other donor–acceptor pair is linked by hexaglycine ($TrpNH_2$–$(gly)_6$–DNS), which is highly flexible and expected to result in a range of Trp–DNS distances. The emission spectra of these peptides are shown in Figure 14.5. The donor is quenched in both D–A pairs, relative to the donor-alone control, $TrpNH_2$–$(gly)_3$–Ac. The donor is more highly quenched in the flexible $(gly)_6$ peptide relative to the rigid $(pro)_6$ peptide. One could use the relative amounts of donor quenching to calculate the D–A distance. This distance would be correct for the rigid peptide $TrpNH_2$–$(pro)_6$–

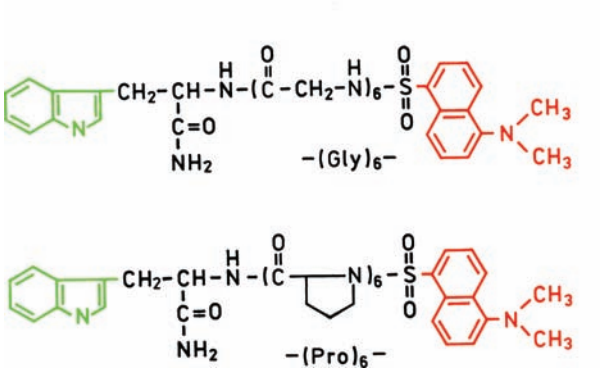

Figure 14.4. Flexible $TrpNH_2$–$(gly)_6$–DNS and rigid $TrpNH_2$–$(pro)_6$–DNS D–A pairs. Revised from [7].

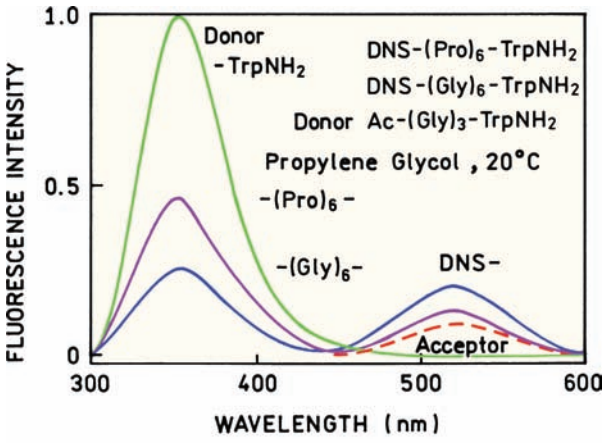

Figure 14.5. Emission spectra of DNS–$(Pro)_6$–$TrpNH_2$ and DNS–$(Gly)_6$–$TrpNH_2$ relative to the donor-alone control Ac–$(Gly)_3$–$TrpNH_2$. Ac refers to an N-acetyl group. Revised from [7].

DNA, but incorrect for the flexible $TrpNH_2$–$(gly)_6$–DNS peptide. For the $(gly)_6$ peptide one must use time-resolved measurements to obtain information beyond a weighted apparent distance.

Information about the distance distribution for flexible molecules can be recovered from the time-resolved decays of the donor. Frequency-domain data for the two D–A peptides (●) and the donor-alone control molecule (○) are shown in Figure 14.6. In the absence of acceptor the donor-alone control molecule displays a single-exponential decay with $\tau_D = 5.27$ ns. For the rigid D–A pair (top) energy transfer decreases the donor decay time, as seen by the shift of the phase and modulation values to higher frequencies. However, the donor decay remains reasonably close to a single exponential, as seen by the visual similarity of the one- and two-exponential fits. As predicted in Figure 14.2, a single D–A distance results in a single-exponential decay of the donor. Close inspection of the FD-intensity decay does reveal some heterogeneity ($\chi_R^2 = 8.1$), which is due to a narrow but finite D–A distance distribution.

A remarkably different donor decay is seen for the flexible D–A pair DNS–$(gly)_6$–$TrpNH_2$. For this case the donor decay cannot be approximated by a single exponential, as seen from the dashed line in Figure 14.6 (lower panel), and $\chi_R^2 = 1254$ for the single-decay-time fit. A single-decay-time fit is equivalent to fitting the donor decay to a very narrow distance distribution (eqs. 14.1 and 14.2). For the flexible peptide, the presence of a range of D–A distances caused the donor decay to become highly non-exponential, the extent of which can be used to determine the distance distribution.

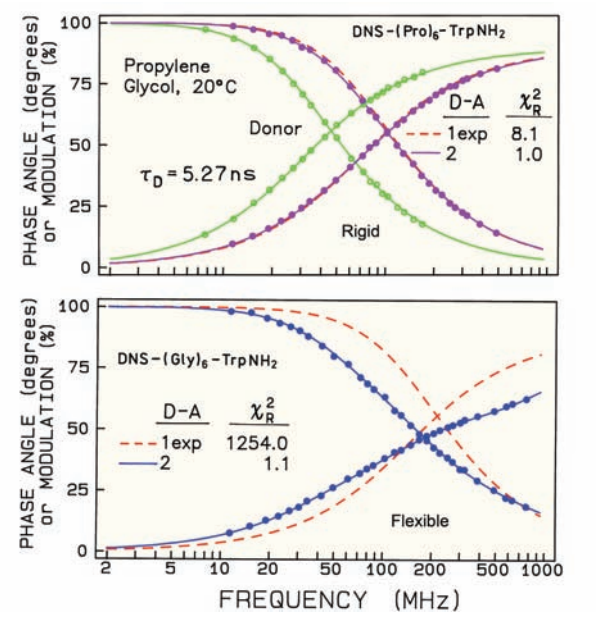

Figure 14.6. Frequency-domain donor intensity decays of DNS–$(pro)_6$–$TrpNH_2$ (top) and DNS–$(Gly)_6$–$TrpNH_2$ (bottom). For the D–A pairs the dashed and solid lines are the best single and double exponential fits, respectively.

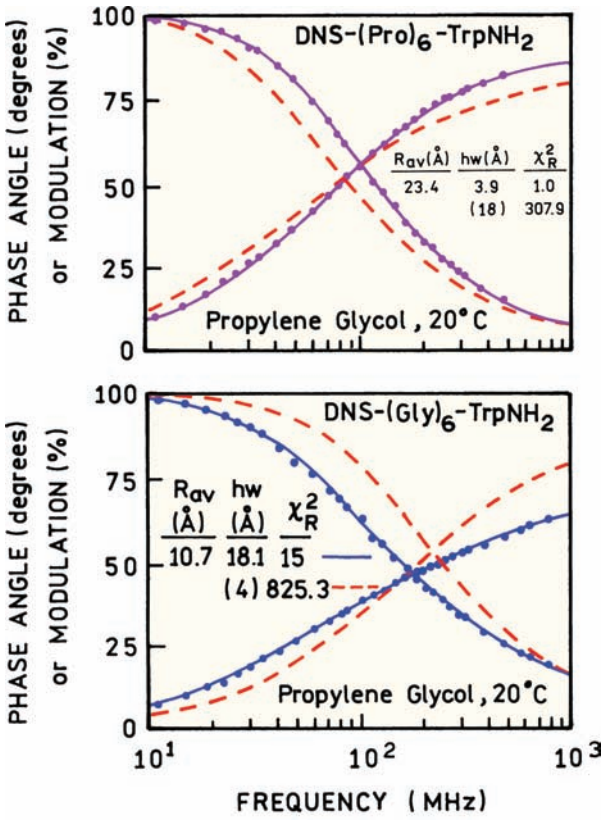

Figure 14.7. Distance-distribution fits to the frequency-domain donor decays for flexible (left) and rigid (right) peptides. The *hw* values in angular brackets (< >) indicate that this value was held constant in the analysis.

The frequency-domain data can be analyzed to recover the distance distribution $P(r)$. This is accomplished by using eq. 14.6 to predict the phase and modulation values for assumed values of $\bar{r}$ and *hw* using the general procedures described in Chapter 4 for time-domain data or Chapter 5 for frequency-domain data. These expressions are shown below (Section 14.4) for the case of single- and multi-exponential donor decays. Analyses of the FD data in terms of the distance-distribution model for both peptides are shown in Figure 14.7. These fits reveal wide and narrow distributions for the flexible and rigid peptides, respectively (Figure 14.8). In this analysis we used the complexity of the donor decays (Figure 14.2, left) to recover the distribution of D–A distances (Figure 14.2, right). The complexity in the donor decay caused by the acceptor (Figure 14.6) was used to determine the probability distribution of acceptors around the donor (Figure 14.8).

14.2.2. Crossfitting Data to Exclude Alternative Models

In addition to obtaining the average distance $\bar{r}$ and half width *hw*, it is important to consider whether the data exclude other distance distributions. This can be accomplished by the procedure of crossfitting the data. This involves using one or more of the parameter values from a second competing model to see if they are consistent with the data. If a competing model also fits the data, then we cannot exclude that model from our consideration without

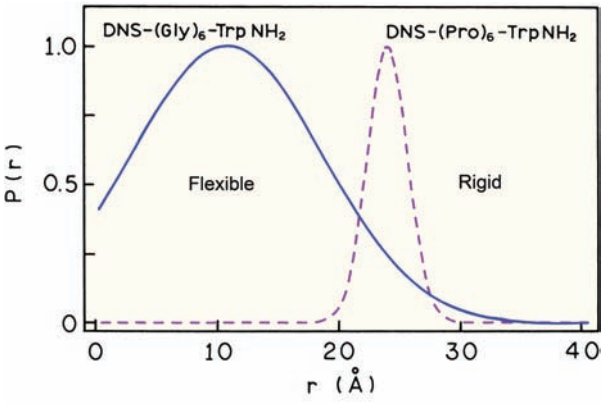

Figure 14.8. Distance–distribution fits for DNS–$(Gly)_6$–$TrpNH_2$ (solid) and DNS–$(pro)_6$-$TrpNH_2$ (dashed). Revised from [7].

additional data. During this fit the mean distance was a variable parameter. For the flexible peptide $TrpNH_2$–$(gly)_6$–DNS the alternative model was tested by attempting to fit the data using the half width of 4 Å found for the rigid peptide. The value of hw = 4 Å is held constant and the least-squares fit run again to minimize χ_R^2 using the flexible peptide data. The dashed line (Figure 14.7, left) shows the data for $TrpNH_2$–$(gly)_6$–Gly are not consistent with a narrow distance distribution. Similarly, the data for $TrpNH_2$–$(pro)_6$–DNA could not be fit with a wide distribution (dashed line, curves in right panel of Figure 14.7). In these cases the attempt to fit the data with different parameter values resulted in obviously unacceptable fits. However, for conformational changes of proteins one can expect the distance distributions to be more similar than for these two hexapeptides, so that the ability to reject similar distributions may be more questionable.

14.2.3. Donor Decay without Acceptor

An important aspect of the distance-distribution analysis is knowledge of the donor decay time. This is typically measured using a control molecule that is comparable to the D–A pair except that it lacks the acceptor (donor-alone molecule). In the case of the two hexapeptides the donor control molecule was $TrpNH_2$–$(gly)_3$–Ac, in which the tryptophan donor was attached to a glycine tripeptide. The tripeptide was acetylated at the N terminus to be more like the D–A pairs and to avoid quenching by the terminal amino group. The amide group does not quench the nearby indole. The selection of a suitably designed donor-alone control molecule is a critical step in any energy transfer experiment. Typically the donor decay time (or decay times for a multi-exponential decay) is measured separately. The data (TD or FD) for the D–A pair are then analyzed while the value of τ_D is held fixed. This is necessary because the donor intensity decays of the D–A pair only provides information when compared to the decay that would be observed without energy transfer.

Depending upon the available software the data for the donor-alone and D–A pairs can also be analyzed simultaneously. In this case the program needs to know that the value(s) of τ_D is determined only by the donor-alone data, as there is no RET in the donor-alone decay. At first glance one may think that this simultaneous analysis is identical to fixing τ_D, and analyzing the data for the D–A pair. In fact, these two methods are different and this second analysis is preferred. If the presence of the acceptor has no effect on the donor decay besides that due to RET, both modes of analysis will yield the same value of τ_D. However, if the presence of the acceptor somehow affects τ_D other than by RET, then the second mode of analysis could reveal this effect. Alternatively, since energy transfer decreases the intensity of the donor, an increased contribution of impurity fluorescence to the data for the D–A pair could result in different values of τ_D for each mode of analysis.

14.2.4. Effect of Concentration of the D–A Pairs

In general, the extent of energy transfer depends on the concentration of the D–A pairs. However, for linked D–A pairs energy transfer is usually dominated by the linked acceptor. For unlinked D–A pairs the acceptor concentration needs to typically be in the millimolar range for significant energy transfer (Chapter 15). This is because mM concentrations are needed to result in one or more acceptor molecules to be within the Förster distance of the donor. Hence, we made no mention of the concentration of the linked D–A pairs in the preceding sections. Knowledge of the concentration was unnecessary because each donor sees an effective constant concentration of the acceptor determined by the length and flexibility of the linker to which the acceptor is attached. However, the concentration of linked D–A pairs should be low enough to avoid inner filter effects and transfer between donors and acceptors on unlinked D–A pairs. Under these conditions, the extent of energy transfer will be independent of the bulk concentration of the D–A pairs.

14.3. DISTANCE DISTRIBUTIONS IN PEPTIDES

The principles described above have been applied to a wide variety of proteins using time or frequency-domain measurements. Time-domain measurements have been used to recover distance distributions in native and unfolded staphylococcal nuclease,[4] troponin C,[8] and cardiac troponin I.[9] This approach was initially described by Haas and coworkers on bovine pancreatic trypsin inhibitor (BPTI). This protein was labeled with a naphthalene donor at the N-terminal amino group, and selectively labeled with a coumarin acceptor on each of its four lysine residues. The labeled BPTI was studied during folding and unfolding to determine the folding pathway. (See Representative Publications on Measurement of Distance Distributions near the end of this chapter for references). Frequency-domain measurements have also been used to measure distance distributions in proteins, including the ribonuclease S pep-

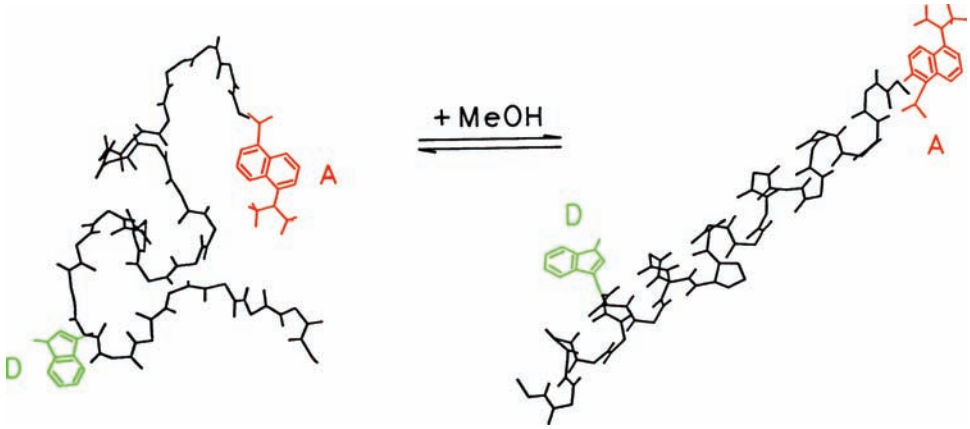

Figure 14.9. Dansyl (acceptor)-labeled melittin in the random-coil and α-helical states. Revised from [23]. Copyright © 1990, with permission from Elsevier Science.

tide,[10] myosin subfragment-1[11], troponin-I,[12] and other peptides and proteins.[13–21] The use of FRET with proteins has been reviewed by Cheung.[22]

14.3.1. Distance Distributions in Melittin

For the purpose of illustrating distance distributions in proteins we have chosen to present data for melittin.[23–24] Melittin has a single intrinsic tryptophan residue as the donor, and was labeled on the N-terminal amino group with a dansyl acceptor. This 26-amino-acid peptide from bee venom was used in Chapter 13 to illustrate measurements of a single D–A distance when in the α-helical state. We now consider melittin in the random-coil state, which folds into a monomeric α-helical state upon addition of methanol (Figure 14.9). This simple peptide illustrates how a change in structure affects the Trp-19 to N-terminal distance.

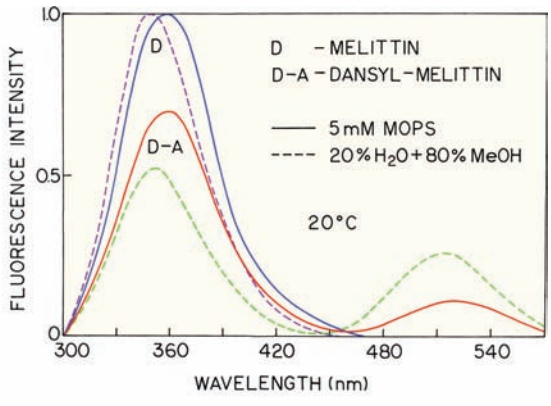

Figure 14.10. Emission spectra of dansyl-melittin in the α-helical and random-coil state. The donor-alone (melittin) intensities are normalized. Reprinted from [23]. Copyright © 1990, with permission from Elsevier Science.

Emission spectra of the donor-alone melittin and dansyl-melittin are shown in Figure 14.10. These spectra show the relative intensities of the D–A pairs relative to the donor without a nearby acceptor. The transfer efficiency can be calculated from these steady-state intensities. The overall efficiency of RET seems to be higher for α-helical melittin in 80% methanol, where melittin is in the α-helical state, than in aqueous buffer (5 mM MOPS), where melittin is in the random-coil state. This difference is seen as a weaker donor emission and stronger acceptor emission (dashed) in 80% methanol. If we calculated a single distance from these data we would conclude that the Trp-to-dansyl distance is smaller in the α-helical state (dashed) than in the random-coil state (solid). However, the time-resolved data yield a different result.

Frequency-domain intensity decays are shown in Figure 14.11 for random-coil melittin, as the donor-alone control (●) and for dansyl-melittin (○). The presence of the acceptor shortens the donor decay time, which is seen as a shift in the donor response to higher frequencies in the presence of acceptors. While we expect melittin to be in the random-coil state with a distribution of D–A distance, it is difficult to see increased heterogeneity in the tryptophan decay due to the presence of acceptor in the random-coil state. The similarity of the donor-alone and donor–acceptor frequency responses in Figure 14.11 illustrates the difficulty in determining distance distributions in proteins. Careful analysis is needed not only to recover the distance distributions, but also whether the data are consistent or not with competing models.

Table 14.1. Intensity Decays of Melittin and Dansyl–Melittin[a]

Sample	%MeOH	$\bar{\tau}$ (ns)[b]	γ_i (ns)	α_i	f_i	χ_R^2 1[c]	2	3
Melittin	0	3.29	0.32	0.408	0.065			
			2.49	0.401	0.440			
			4.64	0.191	0.400	548	5.7	1.4
Dansyl-melittin	0	2.41	0.14	0.500	0.064			
			1.12	0.287	0.297			
			3.24	0.213	0.639	733	7.4	2.5
Melittin	80	4.19	0.67	0.374	0.092			
			2.96	0.434	0.468			
			6.29	0.192	0.440	551	7.7	2.8
Dansyl-melittin	80	2.46	0.37	0.345	0.083			
			1.73	0.561	0.631			
			4.69	0.094	0.286	368	9.5	1.2

[a]From [23].
[b]$\bar{\tau}$ is the mean decay time calculating using $\bar{\tau} = f_1\gamma_2 + f_2\gamma_2 + f_3\gamma_3$.
[c]The numbers represent the number of decay times used in the analysis.

Another difficulty in measuring distance distributions in proteins is the presence of multi-exponential decays in the absence of acceptor. The intensity decay of melittin itself is a multi-exponential that requires at least three decay times for a suitable fit in either solvent (Table 14.1). Also shown in Table 14.1 are the multi-exponential analyses for dansyl-melittin in aqueous buffer (random coil) and in 80% methanol (α-helical). The mean decay time ($\bar{\tau}$) of the tryptophan donor is shortened by the presence of acceptor. However, it is difficult if not impossible to interpret these values of α_i and τ_i in terms of the melittin conformation.

The data are best analyzed in terms of a distance distribution (Figure 14.12). In the absence of methanol, the data are consistent with a wide distribution of Trp-to-dansyl distances ranging from 0 to 40 Å. The mean ($\bar{\tau}$) and half width (*hw*) were 17 and 25 Å, respectively. In the presence of methanol the distance distribution becomes quite sharp, with ($\bar{\tau}$) = 25 Å and *hw* = 3 Å (Figure 14.13), which is interpreted as being due to the α-helical structure shown in Figure 14.9.

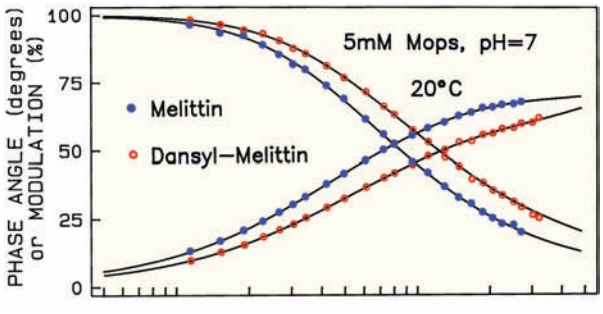

Figure 14.11. Frequency-domain donor decay of melittin (●) and dansyl–melittin (○). Revised from [23]. Copyright © 1990, with permission from Elsevier Science.

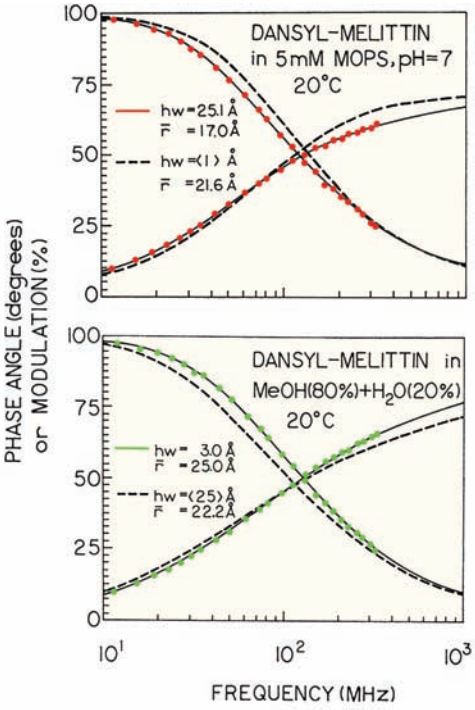

Figure 14.12. Frequency-domain tryptophan decays of dansyl–melittin in the random-coil (top) and α-helical states (bottom). Revised from [23]. Copyright © 1990, with permission from Elsevier Science.

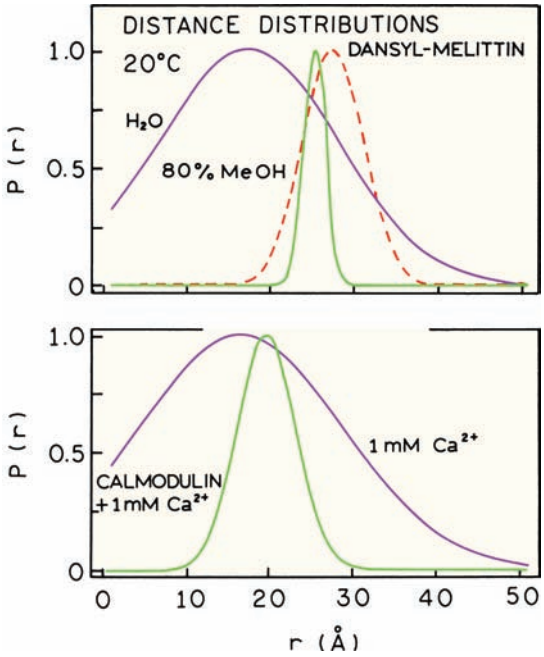

Figure 14.13. Distance distribution of dansyl–melittin in solution and when bound to calmodulin. Revised from [23]. The dashed line (top) shows the distance distribution obtained with consideration Trp-to-dansyl diffusion: $D = 6.5 \times 10^{-6}$ cm^2/s. Revised from [24].

Because of the limited resolution using the time-resolved data it is important to test the uniqueness of the result. This was accomplished by crossfitting the data with alternate parameter values. For instance, the data for the random-coil state are fit to a distribution with a variable mean value but a small half width, which is a fixed parameter. The data for the random-coil state (Figure 14.12, top) are clearly inconsistent with a narrow half width (dashed). The data for the α-helical state (Figure 14.12, bottom) are clearly inconsistent with the half width of the random-coil state (dashed). The visual differences seen in the crossfits makes an important point. If you cannot visually see the difference between the fits of two different models to the data then it is risky to select one result as the correct model.

Distance-distribution analysis can be used to study the conformations of a protein when bound to other biomolecules. In the presence of calcium, calmodulin expresses a hydrophobic patch. When in the α-helical state one side of the melittin helix contains hydrophobic amino-acid side chains that bind to calmodulin. A Trp-to-dansyl distance distribution for melittin was also obtained when bound to calmodulin[24] (Figure 14.13, lower panel). Melittin is expected to be in the α-helical state. Calcium (1 mM) did not affect the melittin distance distribution. However, a relatively narrow distribution was found with 1 mM Ca^{2+} and calmodulin, where binding is expected. It is interesting to notice that the mean distance is somewhat smaller than for the unbound α-helix, suggesting that the hydrophobic patch of calmodulin has imposed some restrictions on the melittin structure. The distance distribution of melittin seems wider when bound to calmodulin than when in solution. There are two possible causes of this result. One is structural heterogeneity in the bound state. The second is the result of using an incorrect model. In Section 14.7 we describe the effects of donor-to-acceptor diffusion for melittin. In fact, the distribution shown for α-helical melittin in Figure 14.13 is narrowed by diffusion, and consideration of this effect results in a somewhat wider distribution for melittin in 80% methanol (Figure 14.13, top, dashed). Donor-to-acceptor diffusion tends to narrow the apparent distance distribution if the analysis is performed without consideration of diffusion.

14.4. DISTANCE-DISTRIBUTION DATA ANALYSIS

14.4.1. Frequency-Domain Distance-Distribution Analysis

It is informative to describe in detail how the frequency domain data for dansyl-melittin were analyzed to recover the distance distribution. A similar approach can be used for analysis of the time-domain data. The first step in any distance-distribution analysis is determination of the intensity decay of the donor alone, followed by use of this decay law in the distance-distribution analysis. For any form of the decay law the phase ($\phi_{c\omega}$) and modulation ($m_{c\omega}$) at a given frequency can be calculated from

$$N_\omega = \frac{\int_0^\infty I(t) \sin \omega t \, dt}{\int_0^\infty I(t) \, dt} \tag{14.7}$$

$$D_\omega = \frac{\int_0^\infty I(t) \cos \omega t \, dt}{\int_0^\infty I(t) \, dt} \tag{14.8}$$

Using these transforms the phase and modulation values can be calculated from

$$\phi_{c\omega} = \arctan(N_\omega / D_\omega) \tag{14.9}$$

$$m_{c\omega} = (N_\omega^2 + D_\omega^2)^{1/2} \tag{14.10}$$

If the donor decay is a single exponential then the decay is given by eq. 14.6, and the transforms are

$$N_\omega = \frac{1}{J}\int_{r=0}^{\infty} \frac{P(r)\omega\tau_{DA}^2}{1+\omega^2\tau_{DA}^2}dr \tag{14.11}$$

$$D_\omega = \frac{1}{J}\int_{r=0}^{\infty} \frac{P(r)\tau_{DA}}{1+\omega^2\tau_{DA}^2}dr \tag{14.12}$$

where the normalization factor J is given by

$$J = \left[\int_0^\infty P(r)\,dr\right]\left[\int_0^\infty I_{DA}(t)\,dt\right] \tag{14.13}$$

In these equations the value of τ_{DA} is given by

$$\frac{1}{\tau_{DA}} = \frac{1}{\tau_D} + \frac{1}{\tau_D}\left(\frac{R_0}{r}\right)^6 \tag{14.14}$$

Hence τ_{DA} depends on distance r, as can be seen from eq. 14.6. The value of τ_{DA} corresponds to the lifetime of the donor for a particular distance r. As was described above, these specific molecules cannot be observed. Only the entire population can be measured, and hence the integrals over r in eqs. 14.11 and 14.12. Analytical expressions for N_ω and D_ω are not available, so these values are calculated numerically. The parameter values describing the distance distribution are recovered from nonlinear least squares by minimization of χ_R^2:

$$\chi_R^2 = \frac{1}{\nu}\sum_\omega \left(\frac{\phi_\omega - \phi_{c\omega}}{\delta\phi}\right)^2 + \frac{1}{\nu}\sum_\omega \left(\frac{m_\omega - m_{c\omega}}{\delta m}\right)^2 \tag{14.15}$$

In this expression ϕ_ω and m_ω are the experimental values, ν is the degrees of freedom, and the subscript c indicates calculated values for assumed values of $\bar{r}$ and hw. The values $\delta\phi$ and δm are the experimental uncertainties in phase and modulation, respectively.

For most proteins or macromolecules the donor-alone decays are not single exponentials. Hence we need to consider how to recover the distance distribution for multi-exponential donors. In this case the donor-alone decays are described by

$$I_D(t) = \sum_i \alpha_{Di}\exp(-t/\tau_{Di}) \tag{14.16}$$

where α_{Di} are the pre-exponential factors and τ_{Di} the decay times for the donor in the absence of any acceptor. This expression was written with the factor I_D^0 because this factor cancels in the frequency-domain analysis. At this point we need to make some assumptions. What are the transfer rates and/or Förster distances from each component in the donor decay? Equation 14.2 gives the decay rate for a fluorophore with a single decay time τ_D. Hence it seems reasonable to assume that the transfer rate for each decay time component is given by

$$k_{Ti}(r) = \frac{1}{\tau_{Di}}\left(\frac{R_0}{r}\right)^6 \tag{14.17}$$

and that the distance-dependent donor decay times are given by

$$\frac{1}{\tau_{DAi}} = \frac{1}{\tau_{Di}} + \frac{1}{\tau_{Di}}\left(\frac{R_0}{r}\right)^6 \tag{14.18}$$

This assumption seems to yield reasonable results, but the assumption has not been proven to be correct. Other assumptions are possible,[25] but do not seem to alter the results. Assuming eq. 14.17 correctly describes the transfer rate from each component, the intensity decay of D–A pairs spaced at a distance r is given by

$$I_{DA}(r,t) = \sum_i \alpha_{Di}\exp\left[-\frac{t}{\tau_{Di}} - \frac{t}{\tau_{Di}}\left(\frac{R_0}{r}\right)^6\right] \tag{14.19}$$

and the intensity decay of the entire sample with many D–A pairs is given by

$$I_{DA}(t) = \int_0^\infty P(r)I_{DA}(r,t)\,dr \tag{14.20}$$

The sine and cosine transforms are

$$N_\omega^{DA} = \frac{1}{J}\int_0^\infty \sum_i \frac{P(r)\alpha_{Di}\omega^2\tau_{DAi}}{1+\omega^2\tau_{DAi}^2}dr \tag{14.21}$$

$$D_\omega^{DA} = \frac{1}{J}\int_0^\infty \sum_i \frac{P(r)\alpha_{Di}\tau_{DAi}}{1+\omega^2\tau_{DAi}^2}dr \tag{14.22}$$

where J is given by eq. 14.13 using the multi-exponential decay law. It is important to notice that a multi-exponential decay for the donor does not introduce any additional parameters into the analysis. This is because the intrinsic decays of the donor are measured in a separate experiment,

using samples without acceptor. The data from the donor are fit to the multi-exponential model, and the parameters (α_{Di} and τ_{Di}) are held constant in eqs. 14.21 and 14.22 during the least-squares analysis. It should be remembered that τ_{DAi} depends on distance (eq. 14.18).

14.4.2. Time-Domain Distance-Distribution Analysis

The procedure for the distance distribution from the time-domain data is analogous to that used for the frequency-domain data. The intensity at any time is described by eq. 14.6. This decay law is used with the convolution integral, and the measured instrument response function $L(t)$, to obtain calculated (c) values of $I_{DA}(t)$ for any given time t_j:

$$I_{DA}^{C}(t_j) = \sum_{k=1}^{j} L(t_k) I_{DA}(t_j - t_k) \Delta t \qquad (14.23)$$

where $I_{DA}(t_j - t_k)$ is given by eq. 14.20. Equation 14.23 can be understood as the intensity at time t_j, being the sum of the intensities resulting from a series of δ-function excitation pulses that in total represents the light pulse $L(t)$.

These calculated values are then compared to the measured (m) data $I_{DA}^{m}(t)$ to minimize χ_R^2. The experimental $I_{DA}^{m}(t)$ data are a convolution of the impulse response function $I_{DA}(t)$ with the instrument function $L(t)$. As for the FD measurements, a separate measurement of the donor decay is needed, and this decay law is held constant in the distance-distribution analysis.

Irrespective of the type of measurement, TD or FD, it should be noted that the limits of the integral (eqs. 14.11 to 14.13) can also be regarded as a variable parameter. Hence one can evaluate if there exists a distance of closest D–A approach (r_{min}) or a maximum D–A distance (r_{max}) that is allowed by the experimental data. If such r_{min} and r_{max} are used then one must be careful to normalize the integrated $P(r)$ function to unity.

It is apparent from the above description (eqs. 14.11–14.22) that the distance-distribution analysis is moderately complex. A flow chart of the analysis may be easier to understand (Figure 14.14). The analysis starts with a model (Förster transfer) and measurements: time-domain or frequency-domain. For the FD data, measured and calculated values of ϕ_ω and m_ω are compared and the parameters varied to minimize χ_R^2. In the case of TD data the calculated values are obtained using eq. 14.23.

When the analysis is completed it is important to determine the uncertainties in the desired parameters. This can be accomplished by analyzing simulated data that contain an amount of noise similar to that in the experimental data, using values of $\bar{r}$ and hw similar to the recovered values. Analysis of such simulated data allows one to determine whether it is possible to resolve the parameters. This is particularly important for similar distributions. We also recommend examination of the χ_R^2 surfaces, which reveal the sensitivity of the data to the described parameters, or the uncertainty range of the parameter values. The use of χ_R^2 surface was discussed in Chapters 4 and 5.

14.4.3. Distance-Distribution Functions

Several different mathematical functions have been used to describe donor-to-acceptor distributions. The Gaussian distribution (eq. 14.5) has been most commonly used. This distribution has been multiplied by different elements, $2\pi r$ and $4\pi r^2$, to presumably account for different volume elements available to the acceptor. Inverted parabolas and other functions have also been used.[26] These different functions result in different parameter values, but the overall distant-dependent probabilities look similar.[26–27] In general, there is only enough information to recover an estimate of the distribution, and finer details are not resolved. For most purposes the simple Gaussian (eq. 14.5) is adequate and best suited to describe D–A distribution in macromolecules. In some cases bimodal Gaussians have been used to describe a protein in multiple conformational states.[28]

The Lorentzian distribution has also been used,[4] but in our experience results in artificially narrow half widths. This is because the amplitude of a Lorentzian decreases slowly with distance from the $\bar{r}$ value. As a result the half width is determined more by the ability of the time-resolved data to exclude these smaller and larger r values than by the actual width of the distribution. For this reason, half widths determined using a Lorentzian model are invariably smaller than those found using a Gaussian model.

14.4.4. Effects of Incomplete Labeling

In studies of distance distributions, or in any study of energy transfer, it is critically important to consider the extent of labeling, particularly by the acceptors. Most often one will measure the donor decay, and paradoxically this means that it is most important to have complete labeling at the acceptor site. The importance of complete acceptor labeling can

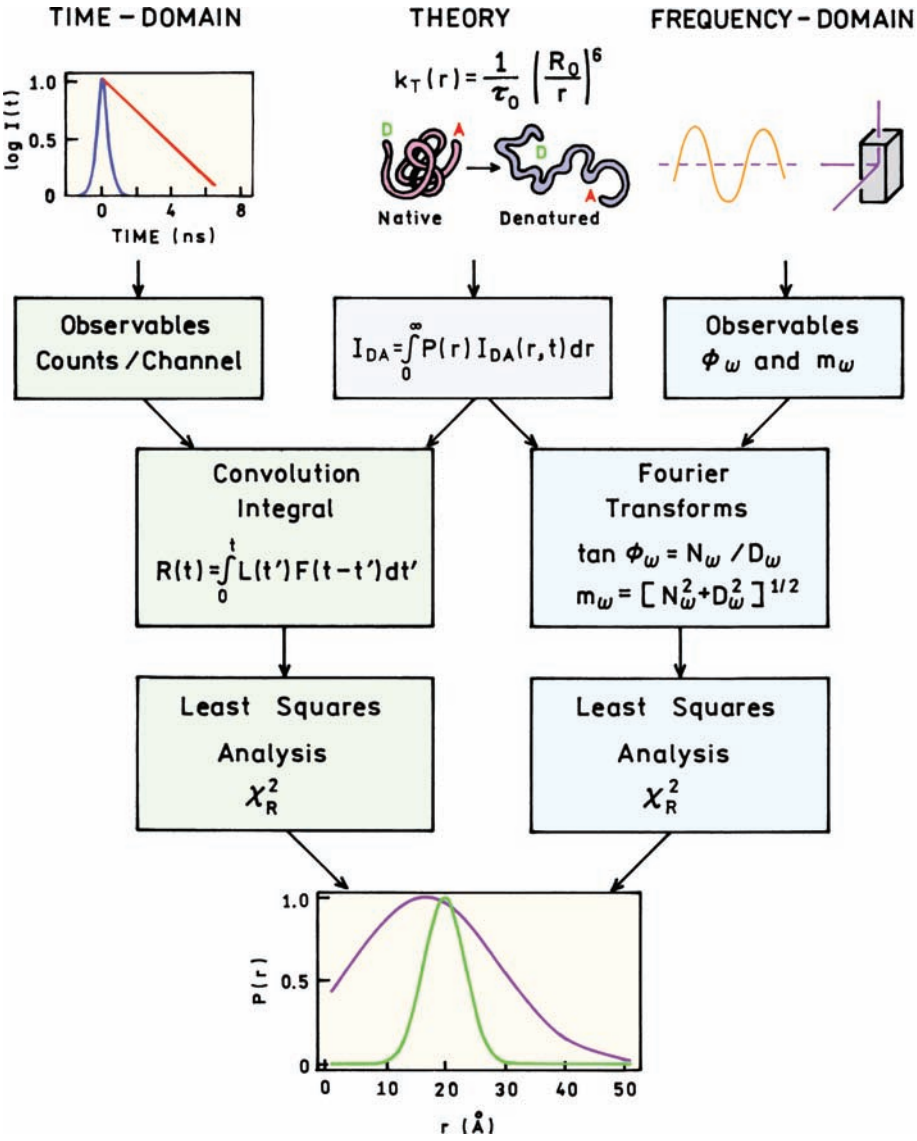

Figure 14.14. Flowchart for distance-distribution analysis.

be understood by considering the effects of incomplete acceptor labeling. This will result in the donor decay containing components due to both the D–A pairs, and from the donors that lack acceptors. The donor-alone molecules contribute to the measured emission greater than their mole fraction. For instance, suppose the donors are quenched tenfold by the linked acceptor, and that 10% of the donors lack acceptors. The donor-alone molecules will contribute tenfold more than their 10% mole fraction, so that the donor-alone signal will be equal to that of the D–A pairs. Hence, a small fraction of underlabeling by acceptors can result in severe distortion of the donor decays. We have found that the presence of a small fraction of donor-alone molecules usually results in a failure of the Gaussian distance-distribution analysis to converge. This is a fortunate occurrence, and preferable to a convergent analysis that may be accepted as correct. We have less experience with the properties of the other distributions in the presence of a significant donor-alone population.

The presence of underlabeling by the acceptor can be accounted for in the least-squares analysis. The donor intensity decay is given by

$$I_{DA}(t) = (1 - f_A) I_D^0 \sum_i \alpha_{0i} \exp(-t/\tau_{Di})$$

$$+ f_A I_D^0 \int_0^\infty P(r) \sum_i \alpha_{Di} \exp\left[-\frac{t}{\tau_{Di}} - \frac{t}{\tau_{Di}} \left(\frac{R_0}{r} \right)^6 \right] \quad (14.24)$$

where f_A is the fraction of the molecules labeled with acceptors.[29–30] While it is possible to correct for acceptor underlabeling, its presence results in decreased information in the donor decay kinetics, and quickly results in loss of resolution about the distance distribution. There seems to be strong correlation between f_A, $\bar{r}$, and hw during the least-squares analysis. If the value of f_A is not known, we regard 5% underlabeling by acceptors as the maximum consistent with reasonable confidence of the distance distribution. If f_A is known, and not a variable in the analysis, then a higher level of underlabeling can be tolerated. Surprisingly, the extent of donor underlabeling is not important in the distance-distribution analysis using the donor emission. Molecules lacking the donor (that is, labeled only with acceptor) do not contribute to the donor decay. The presence of acceptor-only molecules is not important since the solutions are typically too dilute for transfer to acceptors not covalently linked to donors.

14.4.5. Effect of the Orientation Factor κ^2

As described in the previous chapter, the rate of energy transfer depends on the relative orientation of the donor emission dipole and the acceptor absorption dipole. Fortunately, for studies of distance distributions, the effect of κ^2 is likely to be small and use of the dynamic average $\kappa^2 = 2/3$ is reasonable.[31–33] This is because angular displacements of the donor and acceptor result in averaging the value of κ^2 towards 2/3. For a native protein one can expect the donors and acceptors to be relatively immobile during the excited-state lifetime. This is less likely in the random-coil state, where the donor and acceptor, and the peptide itself, can be expected to rotate and diffuse. For molecules the size of fluorophores, the rotational correlation times are typically near 100 ps in water or when located on the surface of a macromolecule. The only mechanism by which κ^2 could affect the distance distribution is if the average D–A orientation were in some way correlated with the D–A distance.[31–32] Given the multitude of conformations accessible to random-coil peptides, this seems unlikely. In general, rotational probe motions occur more rapidly than translational diffusion, so that one can expect rotational averaging even when D–A translational diffusion is minimal. In general, it seems that distance distributions should be largely unaffected by κ^2, especially where the solution is fluid enough to allow segmental motions of the probes relative to the biomolecule.

14.4.6. Acceptor Decays

Information about the distance distribution is also contained in the acceptor decays, so that one may ask why we have stressed measurements of the donor decays. Although in principle either the donors or acceptor decays could be used to recover the distance distribution,[34–35] in most circumstances there is less information in the acceptor decay than in the donor decay. This can be seen by examining the absorption spectra of tryptophan (indole) and dansyl (Figure 13.9). The acceptors typically absorb light at wavelengths used to excite the donors. As a result, the acceptor is excited by two routes: by direct excitation and by RET from the donor. Only the latter portion of the acceptor emission contains information on the distance distribution. Typically, this is the minor fraction of the acceptor intensity, so that most of the acceptor emission is due to the intrinsic decay of the directly excited acceptor. Because of this fact any analysis of the acceptor-decay kinetics must consider directly excited acceptors. Depending on the donor and acceptor emission spectra it may also be necessary to consider contributions of the donor emission at the wavelength chosen to observe the acceptor. In principle an analysis correcting for donor emission and a directly excited acceptor can be performed, but such analyses rarely appear in the literature.

If one can measure the acceptor-decay kinetics due only to RET it will display the unique properties of an excited-state reaction. In the time domain the characteristics of an excited-state reaction are a rise time in the time-dependent intensities, and a negative pre-exponential factor in the multi-exponential analysis. In the frequency domain the phase angles of the acceptor can exceed 90°. These characteristic features are the result of the acceptor being excited by the donor, rather than directly. These features can be hidden by spectral overlap of the donor and acceptor emission spectra and by a directly excited acceptor.

14.5. BIOCHEMICAL APPLICATIONS OF DISTANCE DISTRIBUTIONS

14.5.1. Calcium-Induced Changes in the Conformation of Troponin C

Troponin C (TnC) is one of several proteins involved in muscle contraction. The structure of troponin C in solution is known to be sensitive to calcium. The structure of troponin C consists of two domains linked by a helical peptide (Figure 14.15).

Troponin C typically lacks tryptophan residues. This is fortunate because it allows insertion of tryptophan donors at any desired location by site-directed mutagenesis. In the mutant shown in Figure 14.15 a single-tryptophan residue was placed at position 22 to serve as the donor. As is typical in the design of mutant proteins, the tryptophan (W) was a conservative replacement for phenylalanine (F). A uniquely reactive site for the acceptor was provided by replacing asparagine 52 with a cysteine residue (N52C). This site was labeled with IAEDANS.

The upper panel in Figure 14.16 shows the time-dependent donor decays of the donor-alone and the donor-acceptor protein in the absence of bound calcium.[8] Without acceptor the intensity decay of trp-22 is close to a single exponential. The intensity decay of trp-22 becomes strongly heterogeneous in the presence of IAEDANS acceptor at position 52. This change in the donor decay was used to recover the trp-to-IAEDANS distance distribution, which is seen to be centered near 11 Å and to be about 10 Å wide (Figure 14.17). The close D–A distance and relatively wide distribution comprise one reason for the strongly heterogeneous intensity decay. Close inspection of Figure 14.16 shows that at longer times the intensity decay of the D–A pair is the same as the donor-only protein. This is due to less than 100% labeling by the acceptor. The extent of acceptor labeling is claimed to be about 95%. Because the donor is strongly quenched by the nearby acceptor, even 5% donor-alone protein contributes significantly to the measured intensity decay. The distance distribution shown in Figure 14.17 was corrected for acceptor underlabeling. The data in Figure 14.16 illustrates how only a small amount of donor-alone molecules can distort the data. Complete labeling by

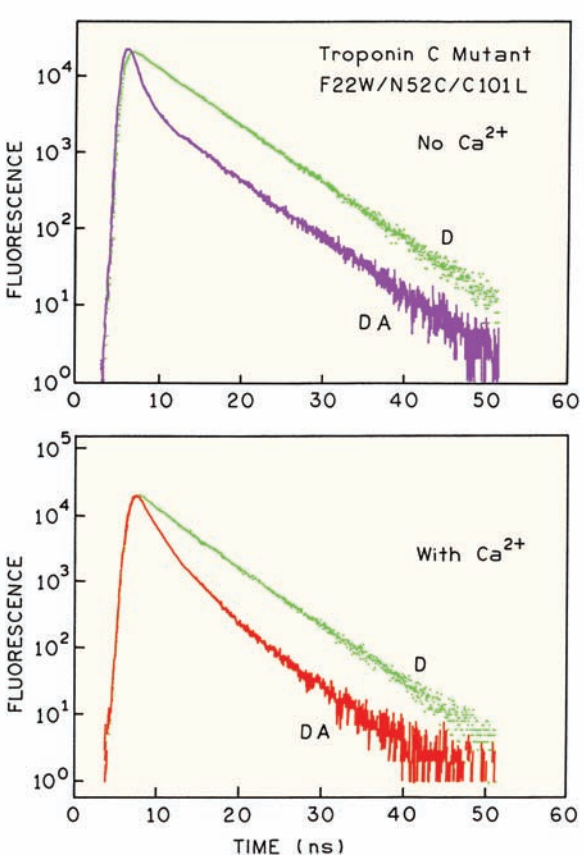

Figure 14.16. Tryptophan-22 intensity decays of Troponin C without (D) and with (DA) an IAEDANS on cysteine 52. Top, without Ca^{2+}. Bottom, with Ca^{2+}. From [8].

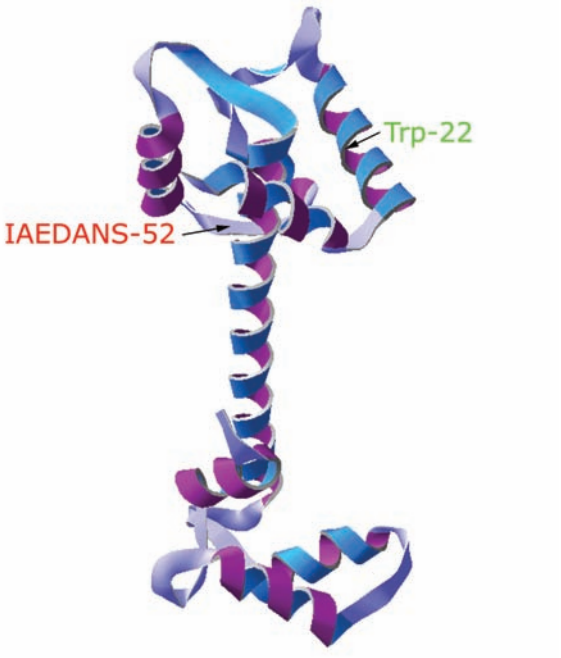

Figure 14.15. The crystal structure of turkey skeletal 2Ca–Troponin C.

Table 14.2. Tryptophan Intensity Decays in Troponin C F22W/N52C/C101L[8]

	τ_1 (ns)	$\alpha_1(f_1)$[a]	τ_2 (ns)	$\alpha_2(f_2)$	τ_3 (ns)	$\alpha_3(f_3)$	χ_R^2
Donor-alone	5.74	1.00					1.4
	5.27	0.58	6.3	0.42			1.6
Donor-acceptor	1.81	1.0					192.3
(R_0 = 22.1 Å)	5.60	0.08	0.76	0.92			1.5
	5.74	0.07	1.28	0.26	0.50	0.67	1.3
		(0.39)[a]		(0.29)		(0.32)	
Donor-alone + Ca^{2+}	4.81	1.0					2.7
	5.39	0.59	3.56	0.41			1.1
Donor-acceptor+Ca^{2+}	2.29	1.0					31.8
(R_0 = 23.9 Å)	4.06	0.18	1.59	0.82			1.9
	5.16	0.06	2.18	0.57	0.79	0.37	1.2
		(0.17)		(0.67)		(0.16)	

[a]Values in parentheses are the fractional intensities calculated from $f_1 = \alpha_1\tau_1/\Sigma_j\alpha_j\tau_j$.

acceptor is perhaps the most important step in measuring a distance distribution.

Binding of calcium to the troponin C mutant results in a substantial change in the intensity decay (Figure 14.16, bottom). When the protein contains bound calcium the decay of trp-22 appears to be mostly a single exponential in the absence of acceptors. The presence of acceptor results in a decrease in donor lifetime, and its decay is no longer a single exponential. The heterogeneity due to acceptor appears to be less than observed in the absence of Ca^{2+}. Analysis of the data in terms of a distance distribution results in a calcium-dependent increase in the D–A distance, and a restriction to a narrow range of distances (Figure 14.17). These results suggest that troponin C adopts a more rigid and/or more unique structure in the presence of calcium.

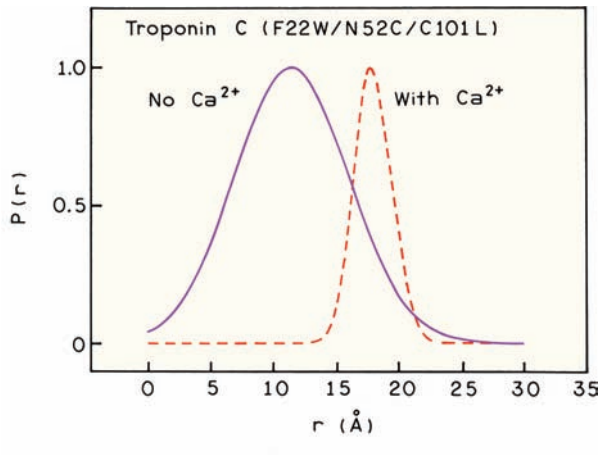

Figure 14.17. Trp-22 to IAEDANS-52 distribution in skeletal muscle TnC mutant (F22W/N52C/C101L) in the absence (solid) and presence (dashed) of bound calcium. From [8].

It is informative to examine the multi-exponential analyses of the donor decays (Table 14.2). In the absence of acceptor the tryptophan decays are close to single exponentials, especially in the absence of Ca^{2+}. In the presence of the IAEDANS acceptor the intensity decay becomes strongly heterogeneous. The extent of heterogeneity can be judged from the χ_R^2 value for the single-decay-time fits. The wider distribution in the absence of Ca^{2+} results in a higher value of χ_R^2 = 192 than in the presence of Ca^{2+} (χ_R^2 = 32), where the distribution is more narrow. The intensity decays in the absence and presence of Ca^{2+} reveal components with decay times close to that of the donor alone. The α_i values typically represent the molecular fraction of the molecules that display their respective decay time. This suggests that 6 to 7% of the TnC molecules lack a bound acceptor, in agreement with the known extent of labeling.[8]

The fractional intensities of each component (f_i values) represent the fractional contributions to the steady-state intensity or the time-integrated intensity decay. The fractional intensity of the component with the donor-alone decay time is nearly 39% in the absence of Ca^{2+}, and 17% in the presence of Ca^{2+}. The larger fractional contribution in the absence of Ca^{2+} is due to the larger extent of energy transfer and a resulting increased contribution of the donor-alone molecules. This large contribution (39%) of the donor-alone molecules, when present at a molecular fraction of 7%, illustrates how the data from strongly quenched samples are easily corrupted by small impurity contributions or underlabeling by the acceptor.

These results illustrate the usefulness of time-resolved measurements for detecting conformational heterogeneity in proteins. The short decay times of the tryptophan residues do not allow time for the conformation to be averaged during the excited-state lifetime, so that the individual conformations contribute to a complex donor decay. This is a somewhat unique feature of fluorescence, as most physical methods reveal an average conformation.

As a final point we wish to stress the importance of time-resolved data for measuring a single distance as well as for measuring distance distributions. If one measures only the steady-state intensities, then one cannot detect the presence of unlabeled or underlabeled molecules. It is easy to be misled by steady-state data that satisfy preconceived notions about the system. In contrast, the time-resolved donor decays contain more information, and will often

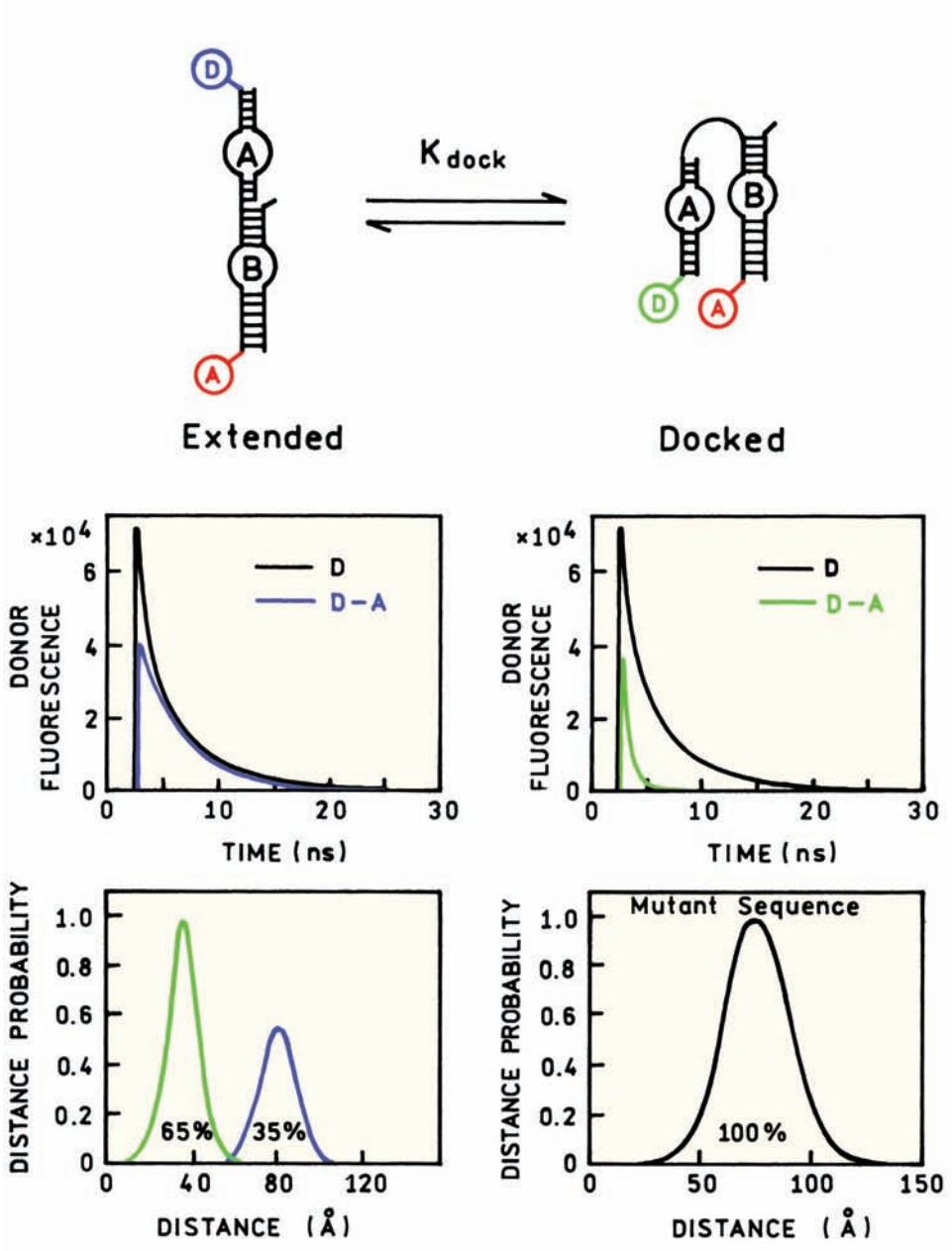

Figure 14.18. Time-resolved donor decays and D–A distance distribution for the hairpin ribozyme. In the lower panels the left side shows the D–A distributions for the native sequence, and the right side for a single G to A mutation. Revised from [36].

reveal inconsistencies due to incomplete labeling, multiple labeling or impurity fluorescence. For this reason measurement of the time-resolved donor decays is recommended for all distance measurements.

14.5.2. Hairpin Ribozyme

In the previous chapter we saw how steady-state RET measurements could be used to study folding of the hairpin ribozyme. Time-resolved measurements provide additional detail on this conformational change.[36–37] Figure 14.18 shows a schematic of the docking motion of this ribozyme. Time-resolved measurements show that the donor decay is more rapid in the docked conformation than in the extended conformation. These decays were used with eqs. 14.18 and 14.20 to recover the distribution of D–A distances. These results confirm that the D–A distance is smaller in the docked conformation. However, in either the extended or docked conformation there is a distribution of D–A distances rather than a single distance. Time-resolved RET was also used to determine the effects of mutations in the hairpin sequence on its conformation. A single mutation near the junction site prevented the docking reaction and resulted in a single wide distribution apparently due to a flexible extended conformation (lower right). See Representative Publications on Measurement of Distance Distributions (near the end of this chapter) for additional references related to RET studies of ribozyme structure.

14.5.3. Four-Way Holliday Junction in DNA

Genetic recombination involves exchange of homologous strands between two duplex DNA molecules. This process occurs at a four-way branch point called a Holliday junction (Figure 14.19). This is a mobile structure that can propagate along the DNA strands. These sites are ultimately removed by cellular enzymes, yielding either the parental or recombinant DNA product. Time–resolved energy transfer has been used to study such junctions.[38-41]

The DNA sequence and sites of labeling of one Holliday junction are shown in Figure 14.19.[39] The strands were labeled on the 5' ends with either fluorescein or rhodamine to provide D–A pairs between sites I and IV. Examination of the oligonucleotide sequence suggests a rather symmetric structure. However, the time-resolved data reveal different rates of energy transfer when the donor (F) and acceptor (R) are on sites I and II or sites I and IV. The data suggest that sites I and II are further apart than sites I and IV

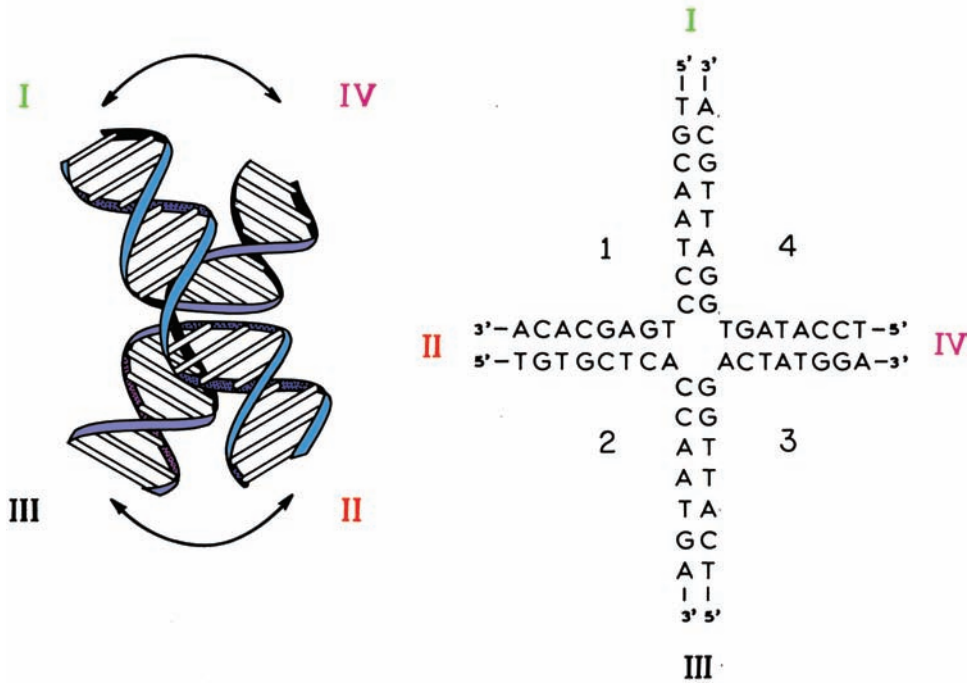

Figure 14.19. DNA Holliday junction. Right: nucleotide sequence; left: solution structure. The 5' ends of each strand contain an aminohexyl moiety for covalent attachment of donor and acceptor dyes. Revised and reprinted with permission from [39]. Copyright © 1993, American Chemical Society.

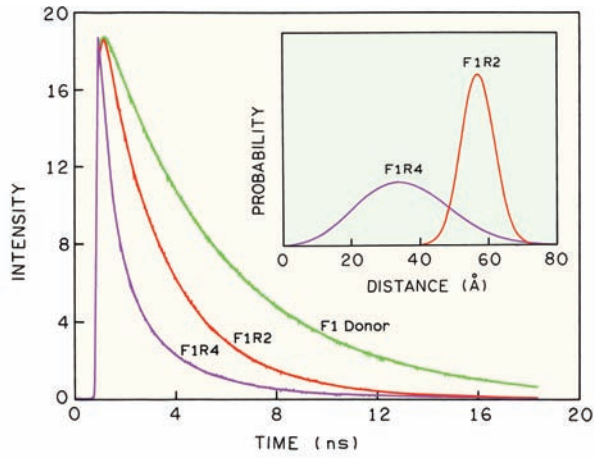

Figure 14.20. Intensity decays and distance distributions in a DNA Holliday junction. Data revised and reprinted with permission from [39]. Copyright © 1993, American Chemical Society.

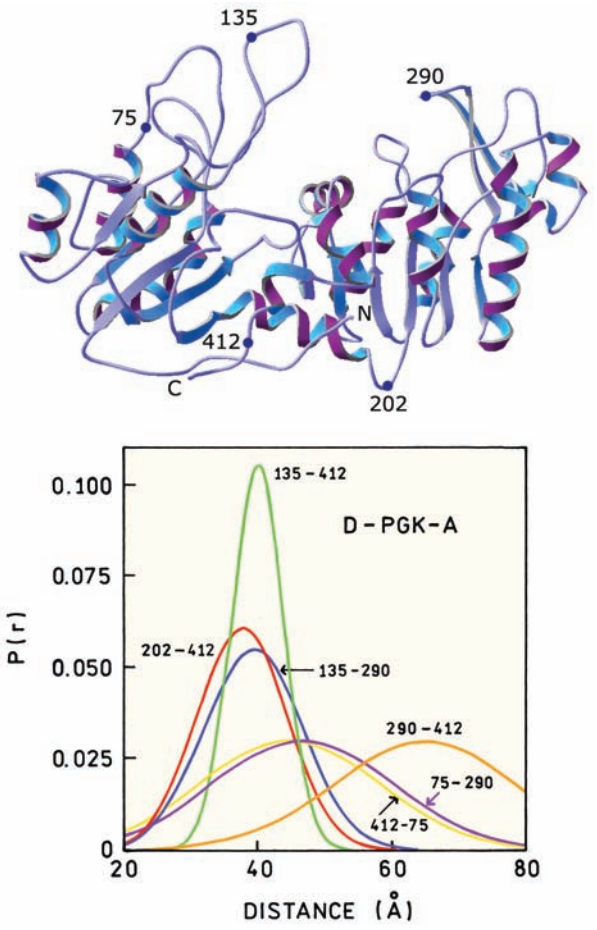

Figure 14.21. **Top**: Structure of PGK showing the sites of cysteine insertion. **Bottom**: Distance distributions recovered between various sites on PGK. Revised and reprinted with permission from [43]. Copyright © 1997, American Chemical Society.

(Figure 14.20). This expectation is confirmed from the recovered distance distributions. There is a narrow distance distribution between one pair of ends and a wide distribution between the other pair of ends (Figure 14.20). Results from other laboratories have suggested somewhat different structures.[40] Nonetheless, these data for a complex macromolecular assembly illustrate how resolution of distance distributions from the time-resolved energy transfer data has become a widely used tool in structural biology. These results on the ribozyme and Holliday junction represent just two examples of a number of studies of distance distribution in nucleic acids and DNA structure (see Representative Publications on Measurement of Distance Distributions).

14.5.4. Distance Distributions and Unfolding of Yeast Phosphoglycerate Kinase

Time-resolved RET was used to measure the distance distributions between a number of sites on phosphoglycerate kinase (PGK), which consists of a single peptide chain with two domains (Figure 14.21).[42–43] A number of single- and double-cysteine mutants were made to provide sites for

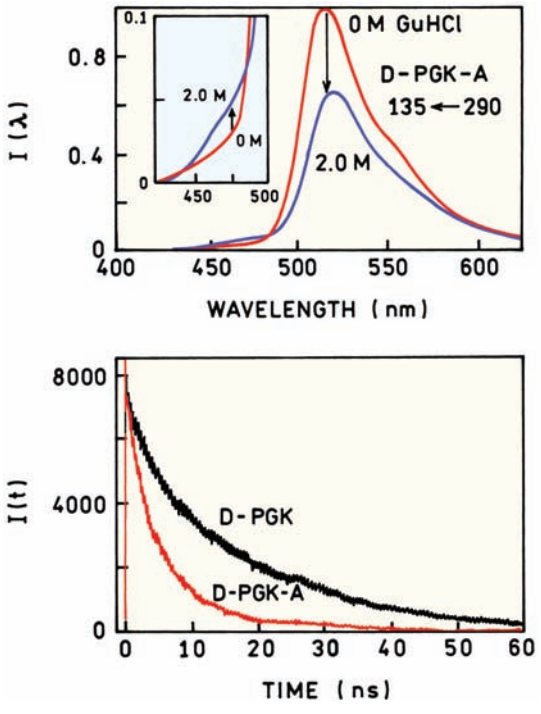

Figure 14.22. **Top**: Emission spectra of D–PGK–A, 135–290, in 0 and 2 M GuHCl. **Bottom**: Time-resolved decay of donor D-PGK and donor–acceptor D–PGK–A, 135–290. Revised and reprinted with permission from [43]. Copyright © 1997, American Chemical Society.

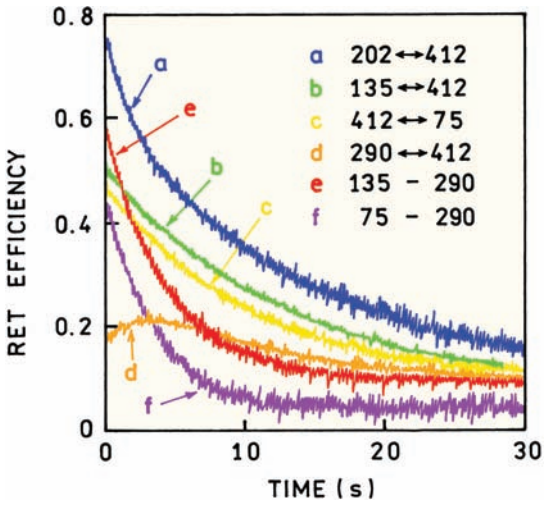

Figure 14.23. Unfolding of donor- and acceptor-labeled PGK in 1.23 M GuHCl. Revised and reprinted with permission from [42]. Copyright © 1997, American Chemical Society.

labeling with an IAEDANS donor and/or an IAF acceptor. The labeling and purification had to be performed carefully to obtain protein that was labeled with both the donor and acceptor, and not doubly labeled with the same fluorophore.[44] The emission spectra of the doubly labeled protein (Figure 14.22) shows a difficulty often encountered with RET measurements, which is observation of the donor or acceptor without contributions from the other fluorophore. In this case the fluorescein emission centered at 515 nm is more intense than the donor emission. Careful selection of emission filters was needed to isolate the relatively small intensity of the donor centered near 470 nm. For this mutant, energy transfer from the IAEDANS donor to the fluorescein acceptor decreases in the presence of 2 M guanidine hydrochloride (GuHCl).

The lower panel in Figure 14.22 shows the time-resolved decays of the donor alone and the D–A pairs for transfer between residues 135 and 290. These decays and other time-resolved donor decays were used to recover the distance distributions between the six sites on PGK (Figure 14.21, lower panel). In some cases the distribution is narrow, and for other D–A pairs the distribution much wider. It is not completely clear if the different distribution widths are due to regions of disorder in the native proteins or differences in the resolution of the time-resolved measurements. The mean distances between the D–A sites were consistent with the crystal structure of the protein.

Since the base-pair sequence of the human genome is known, the amino-acid sequences of many gene products are also known. However, it is generally not possible to predict the three-dimensional structure of a protein from its amino-acid sequence. There is interest in learning the folding pathways of proteins to gain some predictive ability. The PGK mutants shown above were used to study the unfolding pathway of PGK (Figure 14.23).[42] These experiments were performed by mixing folded PGK with GuHCl in a stopped-flow apparatus. To calculate these RET efficiencies it was necessary to measure the donor intensity in the match pairs D-PGK and D-PGK-A (not shown). Examination of the time-dependent RET efficiencies shows that some D–A pairs separate more quickly than others, and that one D–A pair may move together slightly during the unfolding process. These data, and the known labeling sites, can be used to partially determine the pathway PGK takes during the unfolding process.

14.5.5. Distance Distributions in a Glycopeptide

Whereas fluorescence is widely used to study proteins, membranes, and nucleic acids, there are relatively few studies of polysaccharides.[45–48] This is because it is difficult to obtain polysaccharides with a homogeneous structure, and even more difficult to obtain polysaccharides labeled with donor and acceptor fluorophores. Complex oligosaccharides are found in many glycoproteins, including antibodies, hormones, and receptors, yet little is known about their solution conformation. Time-resolved RET was used to resolve the complex conformational distributions of an oligosaccharide.[45] An oligosaccharide was labeled with a naphthyl-2-acetyl donor and a dansylethylenediamine acceptor at one of three locations (Figure 14.24). The authors used both time-resolved and steady-state measurements of RET. The steady-state data provide an important control in all energy transfer measurements. The transfer efficiency determine from the steady-state and time-resolved data should be the same. If not, something is wrong with the sample or analysis. Three donor and acceptor-labeled oligosaccharides were studied, and the data resulted in the resolution of the multiple conformations existing in aqueous solution (Figure 14.25). The Lorentzian model was used to describe the distance distributions. The distance distributions of two of the acceptor sites were bimodal, suggesting that the oligosaccharide branch could fold back toward the donor site. In contrast, the central branch existed in only one conformation and was unable to fold back towards the donor (Figure 14.25).

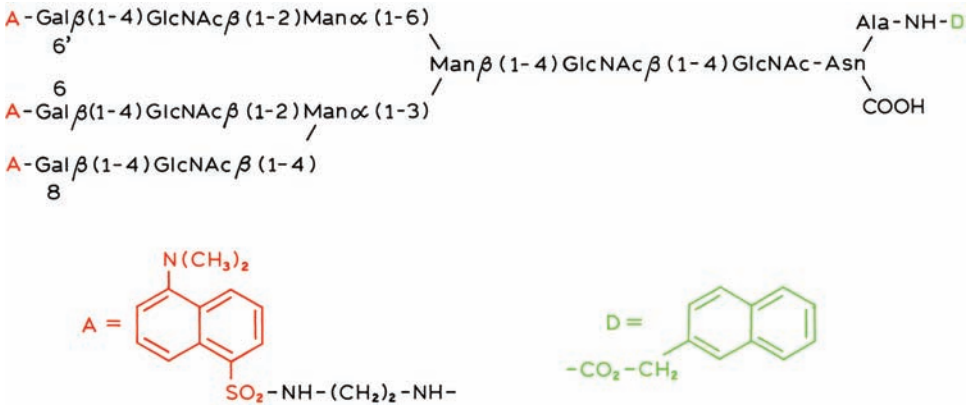

Figure 14.24. Structure of triantennary glycopeptide fluorescence energy-transfer probes. D, naphthyl-2-acetyl; A, dansylethylenediamine. GP-ADanNap glycopeptides all contain D and either A6', A6, or A8. Only one acceptor is present during RET measurements. Revised and reprinted with permission from [45]. Copyright © 1991, American Chemical Society.

14.5.6. Single-Protein-Molecule Distance Distribution

Advanced Topic

The observation of distance distributions in the ensemble measurements of proteins or nucleic acids implies that the individual molecules have different D–A distances. If the individual molecules could be observed then it should be possible to detect differences in RET efficiencies. Single-molecule detection (SMD) is possible under favorable optical conditions for high-quantum-yield fluorophores (Chapter 23). Figure 14.26 shows the structure of a 64-amino-acid fragment of a chymotrypsin inhibitor labeled with a TMR donor and a Cy5 acceptor. A dilute solution of this peptide was observed using an instrument designed for SMD. The excitation was a focused laser beam. As the molecule diffused in and out of the laser beam there were bursts of photons from the donor and acceptor. The relative number of donor and acceptor photons was used to calculate RET efficiency. These bursts were counted to obtain a histogram of RET efficiencies (Figure 14.26). In 3 M GuHCl the inhibitor was in the native state with a high RET efficiency near 95%. In 6 M GuHCl there was a wide distribution of RET efficiencies indicating a longer average D–A distance and a range of D–A distances. At an intermediate concentration of 4 M GuHCl there is a bimodal distribution of RET efficiencies.

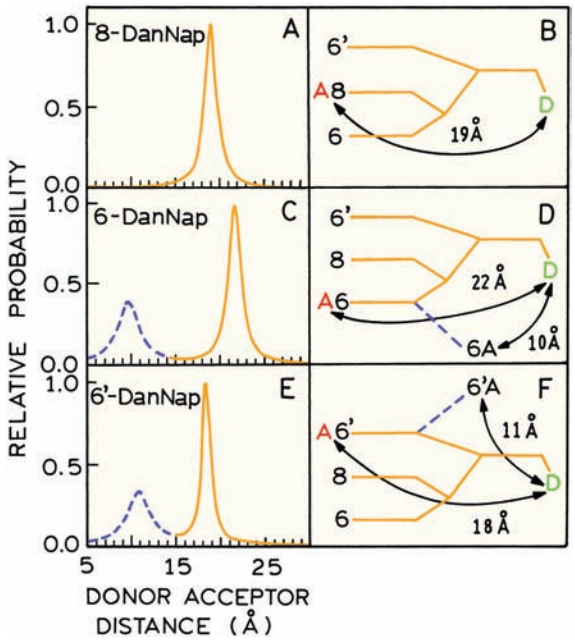

Figure 14.25. Donor/acceptor population distributions. Lorentzian fits of the donor decay curves are shown for GP–8–DanNap, GP–6–DanNap, and GP–6'–DanNap. The ratio of populations for GP–6–DanNap and GP–6'–DanNap were determined to be approximately 60% of the extended conformation and 40% of the folded form. Revised and reprinted with permission from [45]. Copyright © 1991, American Chemical Society.

The RET efficiency histogram in Figure 14.26 shows that folding of the inhibitor is a two-state process. Otherwise there would be a unimodal distribution when the molecule was 50% unfolded. These data also show that the conformations did not interchange within the timescale of the observation, which was about 1 ms for each molecule. It should be noted that these are RET efficiency histograms and not D–A distance histograms, so that the D–A distance decreases along the *x*-axis as the RET efficiency increases.

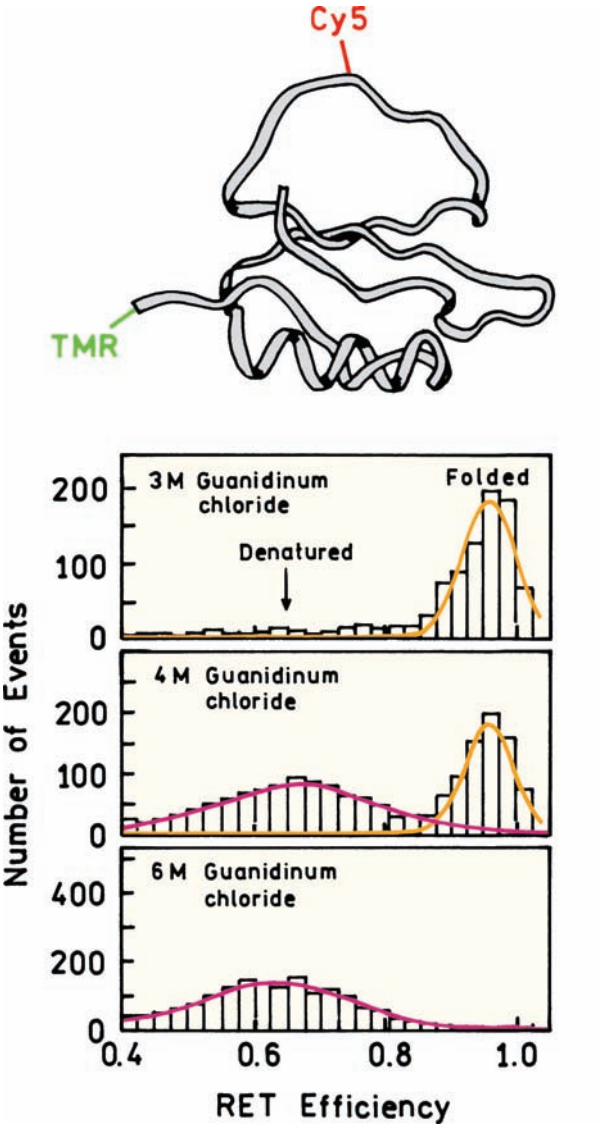

Figure 14.26. Structure of chymotrypsin inhibitor 2 and single-molecule RET efficiencies. Revised from [49].

14.6. TIME-RESOLVED RET IMAGING

RET is beginning to be used with fluorescence-lifetime imaging microscopy (FLIM) to study association reactions in cells.[50–56] This is a promising approach because within reasonable limits the lifetimes can be independent of the local probe concentration. Such measurements require spatially resolved measurements of the donor intensity decays. One approach is to use a streak camera that provides spatial resolution along one axis and time resolution along another. Such measurements are shown for Vero cells in Figure 14.27. The genes for CFP or YFP were fused with the gene

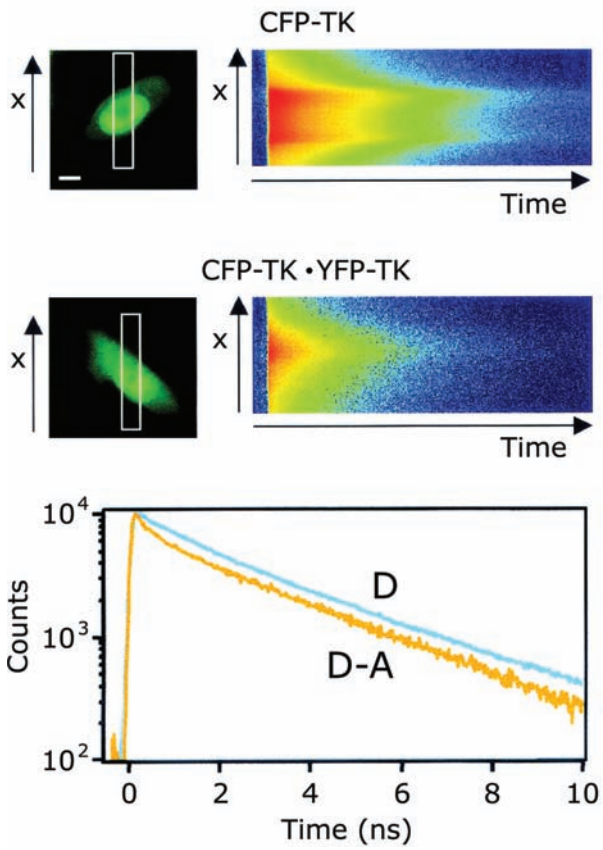

Figure 14.27. Intracellular CFP donor decays for RET between CFP and YFP in Vero cells. CFP and YFP were linked to monomers of thymidine kinase (TK). The transition from red to blue represents decreasing intensity. Revised from [55].

for thymidine kinase (TK) from herpes simplex virus.[55] These two constructs were expressed in Vero cells. The TK monomers form dimers in solution. The goal of the experiment was to detect intracellular dimers. Figure 14.27 shows streak-camera measurements of the CFP-TK donor in the cells. The *x*-axis represents the boxed region across the cells. The top panel shows the decay of the donor in the absence of acceptor, and the middle panel shows the donor decays for a cell transfected with the genes for both CFP–TK and YFP–TK. The CFP donor decays move rapidly in the cell transfected with CFP–TK and YFP–TK than in the cell transfected with only CFP–TK. The lower panel shows the total counts along the *x*-axis. The shape of the decay for the cell with both D and A suggests that a fraction of the CFP–TK is associated with acceptor and a fraction of CFP–TK probably does not have a nearby acceptor. This result is expected because TK forms a homodimer so the cell will contain D–D, A–A, as well as D–A pairs.

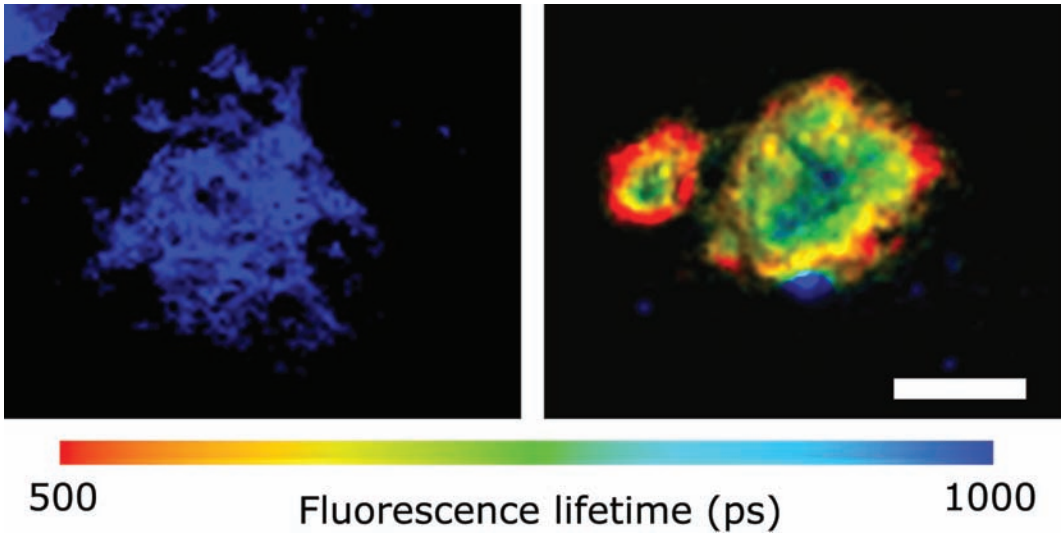

Figure 14.28. FLIM image of senile plaques from a mouse model stained with antibodies specific for the plaque. Left: stained with fluorescein-labeled antibody. Right: stained with both fluorescein-labeled and rhodamine-labeled antibody. Scale bar = 20 μm. Courtesy of Dr. Brian J. Bocskai from Massachusetts General Hospital, Charlestown, MA.

Another example of time-resolved RET imaging is shown in Figure 14.28. The images are of senile plaques, from a mouse model, of the type found in Alzheimer's disease. These images were obtained by staining the plaque with specific antibodies.[56] On the left the plaque was stained with fluorescein-labeled antibody. The lifetime is constant across the plaque. For the image on the right the plaque was stained with two antibodies with the same specificity, one labeled with fluorescein and the other with rhodamine. The fluorescein lifetime is shorter, showing that RET has occurred and that the two types of antibodies are bound near each other on the plaque within the Förster distance. The fluorescein lifetime is not uniform across the plaque, indicating that the antigen density is variable across the plaque. Apparently the antigen density is higher around the edges of the plaque (shorter lifetime) than near the center of the plaque (longer lifetime).

14.7. EFFECT OF DIFFUSION FOR LINKED D–A PAIRS

Advanced Topic

In the preceding sections we considered the donors and acceptors to be static in space and to remain at the same distance during the excited-state lifetime. However, depending on the donor lifetime, and the mutual diffusion coefficient, $D = D_D + D_A$, there can be changes in the D–A distance during the excited-state lifetime (Figure 14.29). For lifetimes from 5 to 20 ns, displayed by most fluorophores, such as $TrpNH_2$–$(gly)_6$–DNS, with τ_D = 4.3 ns (Section 14.2.1), there is little translational displacement, so that the data could be analyzed in terms of a static distance distribution. In more fluid solvents diffusion can influence the extent of energy transfer. The effects of diffusion are complex to calculate, and typically numerical methods are used. We will attempt to illustrate these effects with a minimum of mathematical detail.

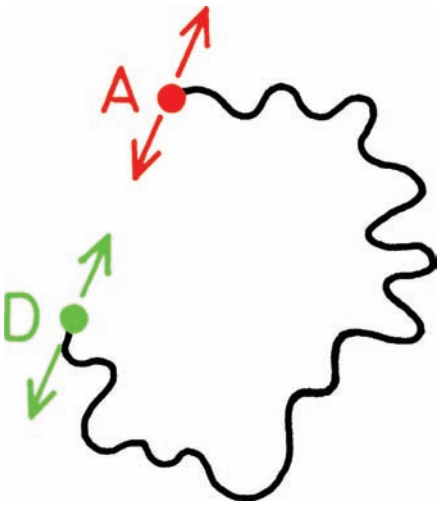

Figure 14.29. Donor–acceptor pair with diffusion.

14.7.1. Simulations of FRET for a Flexible D-A Pair

The effects of D-to-A diffusion on donor decay can be seen from the simulated data for a flexible D–A pair. The excited-state population is given by[3,26]

$$\frac{\partial \overline{N}^*(r,t)}{\partial t} = -\frac{1}{\tau_D}\left[1+\left(\frac{R_0}{r}\right)^6\right]\overline{N}^*(r,t) + \frac{1}{N_0(r)}\frac{\partial}{\partial r}\left(N_0(r)D\frac{\partial \overline{N}^*(r,t)}{\partial r}\right) \qquad (14.25)$$

where $N^*(r,t)$ is the distribution of distances for the excited D–A pairs normalized by time-zero distribution $N_0(r)$. At $t = 0$ the D–A distribution is the equilibrium distribution. However, the distribution changes following excitation due to more rapid energy transfer between the more closely spaced D–A pairs as compared to the more widely spaced D–A pairs. Equation 14.25 is basically the diffusion equation with an added sink term to account for loss of the excited acceptor. The time-dependent intensity decay is given by

$$I_{DA}(t) = I_D^0 \int_{r_{min}}^{r_{max}} P(r)\overline{N}^*(r,t)\,dr \qquad (14.26)$$

where r_{min} and r_{max} are chosen to include the accessible distances. Calculation of $I_{DA}(t)$ in the presence of diffusion is moderately complex, and the details can be found elsewhere.[57–61]

To understand the expected effects of diffusion it is valuable to examine simulated data. Simulated time-domain and frequency-domain data for an assumed donor decay time of 5 ns are shown in Figure 14.30. The distribution of distances at time $t = 0$ was assumed to be a Gaussian, with $\overline{r}$ = 20 Å, hw = 15 Å, and a Förster distance of 25 Å. If the value of D is 10^{-7} cm²/s there is little time for motion during the excited-state lifetime. This can be seen from the near overlap of the simulated data with $D = 0$ and $D = 10^{-7}$ cm²/s. The mean D-to-A displacement $(\Delta x^2)^2$ can be calculated to be $\sqrt{2D\tau_D}$ = 3.2 Å. While significant, this distance is about half the width of a donor or acceptor molecule, and small compared to the assumed $\overline{r}$ = 20 Å. Because of the range of D–A distances the frequency-domain data are spread out along the frequency axis, and the intensity decay is complex (bottom). As the diffusion coefficient increases the intensity decay becomes more rapid, and the frequency response shifts to higher frequency. Both effects are indicative of an increasing amount of energy transfer. It is important to notice that the frequency response becomes more like a single exponential with increasing rates of diffusion. The same effect can be seen in the time-domain data (top). The donor decay becomes more rapid and more like a single exponential as the diffusion coefficient increases. These simulated data show that D–A diffusion increases the extent of energy transfer and alters the shape of the donor intensity decay. Either the FD or TD data can be used to recover the rate of D–A diffusion as well as the distribution of distances.

Why does D–A diffusion result in increased energy transfer? At first glance it seems that diffusion is just as likely to move the donor and acceptor further apart as it is likely to bring them closer together. A more in-depth understanding of diffusion and RET can be obtained by examining the distance distributions in the excited state. The excited-state distributions evolve with time following pulsed excitation. These time-dependent distributions are shown in

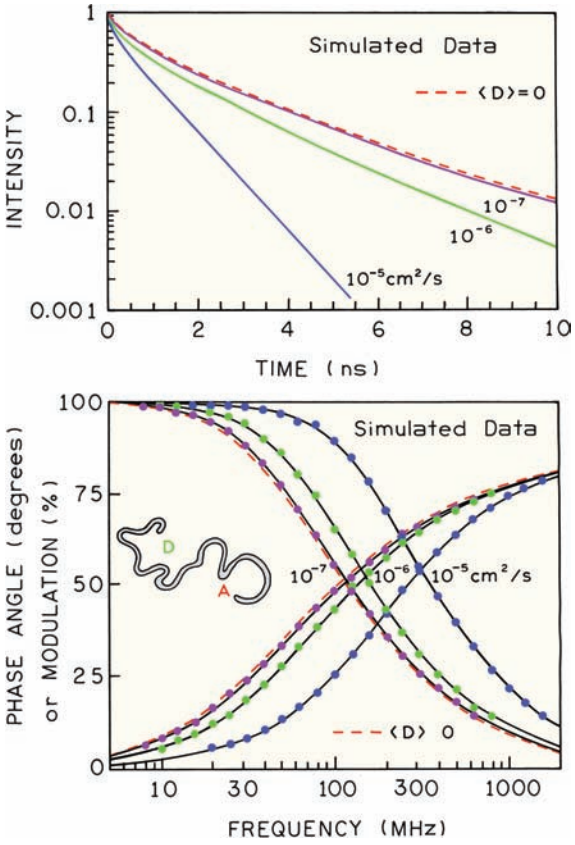

Figure 14.30. Effect of D-to-A diffusion in a linked D–A pair as seen in the time domain and the frequency domain. The dashed line shows the frequency response for $D = 0$. Revised from [58].

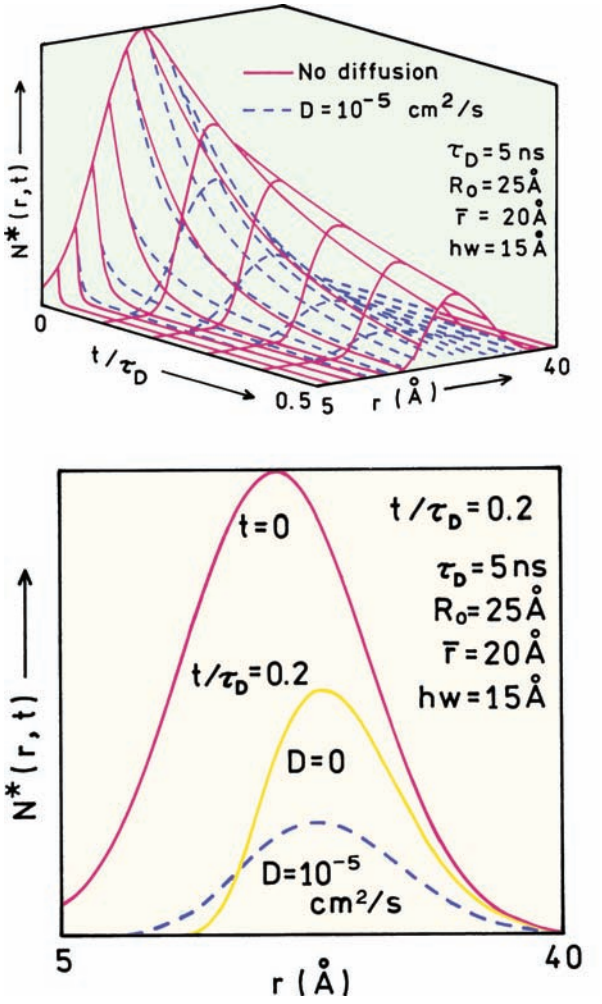

Figure 14.31. Simulated excited-state donor distributions in the absence and presence of diffusion. The assumed parameters values are shown on the figure. Reprinted with permission from [58]. Copyright © 1994, American Society for Photobiology.

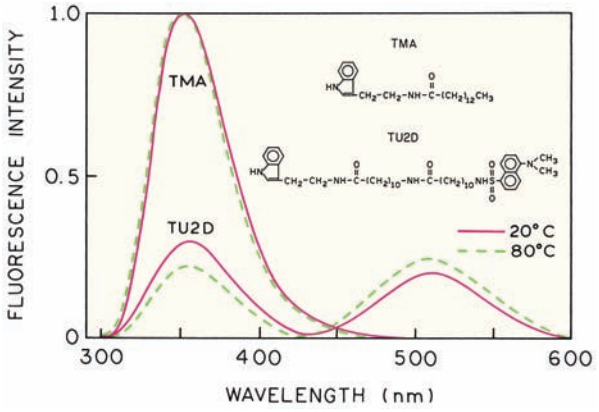

Figure 14.32. Emission spectra of the donor alone (TMA), and of the donor–acceptor pair (TU2D) in propylene glycol from 20 to 80°C. The emission spectra of TU2D are normalized to the intensity of TMA at each temperature.

Figure 14.31 for $D = 10^{-5}$ cm²/s and the same donor lifetime and R_0 as in Figure 14.30. The upper panel shows the entire excited-state population for both time and distance. The donor population decays move rapidly in the presence of diffusion (dashed). The lower panel in Figure 14.31 shows the $P(r)$ distributions at $t = 0$ and $t = 1$ ns, with (dashed) and without diffusion (solid). In the absence of diffusion the excited-state population quickly shifts to longer distances, as shown for $t = 1$ ns, $t/\tau_D = 0.2$. This occurs because the distance dependence of $k_T(r)$ causes the more closely spaced D–A pairs to transfer more rapidly. For rapid D–A diffusion the population of D–A pairs at shorter distances is replenished by diffusion (dashed), and the closely spaced D–A population displays more rapid transfer. This replenishment of the closely spaced D–A pairs by diffusion results in increased energy transfer with increasing rates of diffusion.

14.7.2. Experimental Measurement of D–A Diffusion for a Linked D–A Pair

The role of diffusion in energy transfer is best understood by an example. Figure 14.32 shows the emission spectra for a linked indole–dansyl D–A pair TU2D.[58] The donor-alone control molecule is TMA. This flexible D–A pair was found to have the same distance distribution in propylene glycol irrespective of temperature. The donor is quenched to a greater extent at higher temperatures (dashed) due to D–A diffusion during the excited-state lifetime. During the 6-ns donor lifetime the expected D–A displacement is $\sqrt{2D\tau}$ = 11 Å for a diffusion coefficient near 10^{-6} cm²/s, so there is time for donor and acceptor to approach each other while the donor is excited. This results in an increased rate of energy transfer for each D–A pair, and an overall higher transfer efficiency. The increased extent of energy transfer is also seen from the increased acceptor intensity.

Frequency-domain intensity decays of the donor are shown in Figure 14.33, along with the reconstructed time-dependent decays (top panel). A more rapid decay is seen at higher temperature, and the decay is more like a single exponential. The distance distributions recovered at each temperature are the same, so that the differences in the intensity decays are due to diffusion. Because the extent of diffusion in propylene glycol is minimal at 20°C, the differences in the frequency responses at these two temperatures

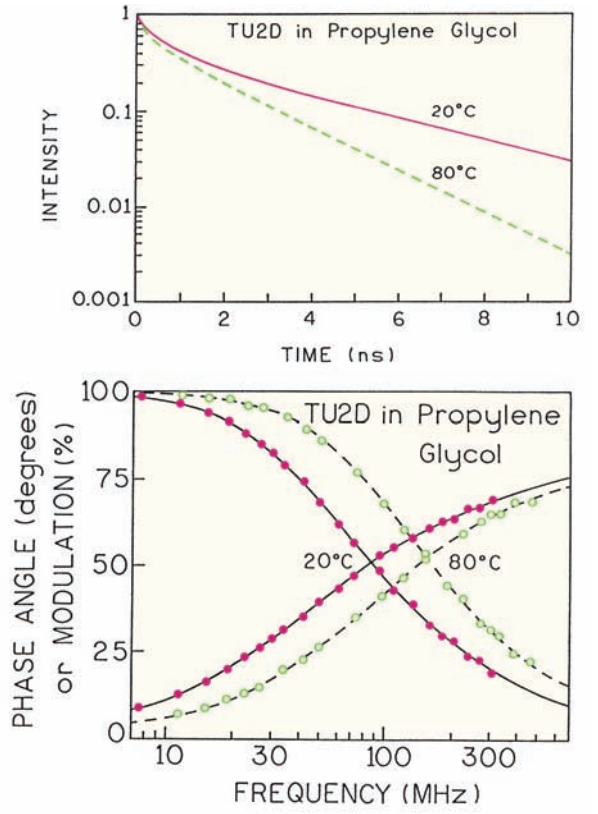

Figure 14.33. Frequency-domain donor decays of TU2D in propylene glycol at 20 and 80°C. The top panel shows the time-dependent decay reconstructed from the FD data. Reprinted with permission from [58]. Copyright © 1994, American Society for Photobiology.

can be regarded as the contribution of diffusion. Clearly D–A diffusion has a significant effect on the FD data.

14.7.3. FRET and Diffusive Motions in Biopolymers

Time-resolved FRET has been proposed as a method to measure domain motions in proteins[62–63] and lateral diffusion in membranes. Motions between domains in proteins are known to occur in many proteins, and are thought to be essential for protein function.[64] Unfortunately, measurements of domain motions in proteins have been largely unsuccessful because of the short decay times of the donors. Diffusion in membranes has only been measured using pyrene derivatives that display decay times over 100 ns.[65–66] From the perspective of protein dynamics, the ns decay times of most fluorophores are too short for measurement of site-to-site motions. However, a few measurements have appeared. Ribonuclease A was studied in a partially unfolded state.[67] In this case the carboxyl terminus was labeled with a naphthylalanine donor that displayed a donor decay time from 25 to 44 ns. The acceptor was a coumarin placed on one of three lysine residues. The time-domain donor decays yielded site-to-site diffusion coefficients of 2 Å^2/ns in the denatured state, but the motions were mostly undetectable in the native state. Similar results were found for a zinc finger peptide, where site-to-site diffusion with D near 10 Å^2/ns was found in the random state, but D decreased to unmeasurable values in the presence of zinc, which induced folding.[15–16] In the case of phosphoglycerate kinase the rate of domain flexing was too slow to allow estimation of the diffusion coefficient with a 20-ns donor lifetime.[63]

14.8. CONCLUSION

In this chapter we have attempted to show the use of time-resolved measurements for determination of the solution conformations of macromolecules. The determination of conformational distributions appears to be a rather unique property of the time-resolved measurements. Most physical methods reveal only an average conformation. Additionally, the data contain information on the timescale of conformational changes. With the introduction of long-lived MLC and lanthanide probes, conformational dynamics will be measurable on timescales from nanoseconds to milliseconds.

As a final comment we want to emphasize that all the results described in this chapter were for covalently linked donor–acceptor pairs, with a single acceptor per donor. Different and somewhat more complex theory is needed to describe systems with multiple acceptors and unlinked probes. Such systems occur commonly in membranes and nucleic acids, which are described in the following chapter.

REFERENCES

1. Haas E, Wilchek M, Katchalski-Katzir E, Steinberg IA. 1975. Distribution of end-to-end distances of oligopeptides in solution as estimated by energy transfer. *Proc Natl Acad Sci USA* **72**:1807–1811.
2. Grinvald A, Haas E, Steinberg IZ. 1972. Evaluation of the distribution of distances between energy donors and acceptors by fluorescence decay. *Proc Natl Acad Sci USA* **69**:2273–2277.
3. Haas E, Katchalski-Katzir E, Steinberg IZ. 1978. Brownian motion of the ends of oligopeptide chains in solution as estimated by energy transfer between chain ends. *Biopolymers* **17**:11–31.
4. Wu P, Brand L. 1994. Conformational flexibility in a staphylococcal nuclease mutant K45C from time-resolved resonance energy transfer measurements. *Biochemistry* **33**:10457–10462.

5. Amir D, Krausz S, Haas E. 1992. Detection of local structures in reduced unfolded bovine pancreatic trypsin inhibitor. *Proteins* **13**: 162–173.
6. Amir D, Haas E. 1986. Determination of intramolecular distance distributions in a globular protein by nonradiative excitation energy transfer measurements. *Biopolymers* **25**:235–240.
7. Lakowicz JR, Wiczk W, Gryczynski I, Johnson ML. 1990. Influence of oligopeptide flexibility on donor–acceptor distance distribution by frequency-domain fluorescence spectroscopy. *Proc SPIE* **1204**:192–205.
8. She M, Xing J, Dong WJ, Umeda PK, Cheung HC. 1998. Calcium binding to the regulatory domain of skeletal muscle troponin C induces a highly constrained open conformation. *J Mol Biol* **281**: 445–452.
9. Dong W-J, Chandra M, Xing J, She M, Solaro RJ, Cheung HC. 1997. Phosphorylation induced distance change in a cardiac muscle troponin I mutant. *Biochemistry* **36**:6754–6761.
10. Maliwal BP, Lakowicz JR, Kupryszewski G, Rekowski P. 1993. Fluorescence study of conformational flexibility of RNase S-peptide: distance-distribution, end-to-end diffusion, and anisotropy decays. *Biochemistry* **32**:12337–12345.
11. Cheung HC, Gryczynski I, Malak H, Wiczk W, Johnson ML, Lakowicz JR. 1991. Conformational flexibility of the Cys 697–Cys 707 segment of myosin subfragment, 1: distance distributions by frequency-domain fluorometry. *Biophys Chem* **40**:1–17.
12. Cheung HC, Wang C-K, Gryczynski I, Wiczk W, Laczko G, Johnson ML, Lakowicz JR. 1991. Distance distributions and anisotropy decays of troponin C and its complex with troponin I. *Biochemistry* **30**:5238–5247.
13. Lakowicz JR, Gryczynski I, Cheung HC, Wang C-K, Johnson ML, Joshi N. 1988. Distance distributions in proteins recovered by using frequency-domain fluorometry: applications to troponin I and its complex with troponin C. *Biochemistry* **27**:9149–9160.
14. Zhao X, Kobayashi T, Malak H, Gryczynski I, Lakowicz JR, Wade R, Collins JH. 1995. Calcium-induced troponin flexibility revealed by distance distribution measurements between engineered sites. *J Biol Chem* **270**(26):15507–15514.
15. Eis PS, Kusba J, Johnson ML, Lakowicz JR. 1993. Distance distributions and dynamics of a zinc finger peptide from fluorescence resonance energy transfer measurements. *J Fluoresc* **3**(1):23–31.
16. Eis PS, Lakowicz JR. 1993. Time-resolved energy transfer measurements of donor–acceptor distance distributions and intramolecular flexibility of a CCHH zinc finger peptide. *Biochemistry* **32**:7981–7993.
17. Bacchiocchi C, Graceffa P, Lehrer SS. 2004. Mysoin-induced movement of αα, αβ, and ββ smooth muscle tropomyosin on actin observed by multisite FRET. *Biophys J* **86**:2295–2307.
18. Miki M, Kouyama T. 1994. Domain motion in action observed by fluorescence resonance energy transfer. *Biochemistry* **33**:10171–10177.
19. Dong WJ, Chandra M, Xing J, She M, Solaro RJ, Cheung HC. 1997. Phosphorylation-induced distance change in a cardiac muscle troponin I mutant. *Biochemistry* **36**:6754–6761.
20. Navon A, Ittah V, Landsman P, Scheraga HA, Haas E. 2001. Distributions of intramolecular distances in the reduced and denatured states of bovine pancreatic ribonuclease A: folding initiation structures in the C-terminal portions of the reduced protein. *Biochemistry* **40**:105–118.
21. Szmacinski H, Wiczk W, Fishman MN, Eis PS, Lakowicz JR, Johnson ML. 1996. Distance distributions from the tyrosyl to disulfide residues in the oxytocin and [Arg^8]-vasopressin measured using frequency-domain fluorescence resonance energy transfer. *Eur Biophys J* **24**:185–193.
22. Cheung HC. 1991. Resonance energy transfer. In *Topics in fluorescence spectroscopy*, Vol. 2: *Principles*, pp. 127–176. Ed JR Lakowicz. Plenum Press, New York.
23. Lakowicz JR, Gryczynski I, Wiczk W, Laczko G, Prendergast FC, Johnson ML. 1990. Conformational distributions of melittin in water/methanol mixtures from frequency-domain measurements of nonradiative energy transfer. *Biophys Chem* **36**:99–115.
24. Lakowicz JR, Gryczynski I, Laczko G, Wiczk W, Johnson ML. 1994. Distribution of distances between the tryptophan and the N-terminal residue of melittin in its complex with calmodulin, troponin C, and phospholipids. *Protein Sci* **3**:628–637.
25. Albaugh S, Steiner RF. 1989. Determination of distance distribution from time domain fluorometry. *J Phys Chem* **93**:8013–8016.
26. Katchalski-Katzir E, Haas E, Steinberg IA. 1981. Study of conformation and intramolecular motility of polypeptides in solution by a novel fluorescence method. *Ann NY Acad Sci* **36**:44–61.
27. Lakowicz JR, Johnson ML, Wiczk W, Bhat A, Steiner RF. 1987. Resolution of a distribution of distances by fluorescence energy transfer and frequency-domain fluorometry. *Chem Phys Letts* **138**(6): 587–593.
28. Kulinski T, Wennerberg ABA, Rigler R, Provencher SW, Pooga M, Langel U, Bartfai T. 1997. Conformational analysis of glanin using end to end distance distribution observed by Förster resonance energy transfer. *Eur Biophys J* **26**:145–154.
29. Lakowicz JR, Gryczynski I, Wiczk W, Kusba J, Johnson ML. 1991. Correction for incomplete labeling in the measurement of distance distributions by frequency-domain fluorometry. *Anal Biochem* **195**: 243–254.
30. Yang M, Millar DP. 1996. Conformational flexibility of three-way DNA junctions containing unpaired nucleotides. *Biochemistry* **35**: 7959–7967.
31. Englert A, Leclerc M. 1978. Intramolecular energy transfer in molecules with a large number of conformations. *Proc Natl Acad Sci USA* **75**(3):1050–1051.
32. Wu P, Brand L. 1992. Orientation factor in steady-state and time-resolved resonance energy transfer measurements. *Biochemistry* **31**:7939–7947.
33. Dos Remedios CG, Moens PDJ. 1995. Fluorescence resonance energy transfer spectroscopy is a reliable "ruler" for measuring structural changes in proteins. *J Struc Biol* **115**:175–185.
34. Beecham JM, Haas E. 1989. Simulations determination of intramolecular distance distributions and conformational dynamics by global analysis of energy transfer measurements. *Biophys J* **55**:1225–1236.
35. Ohmine I, Silbey R, Deutch JM. 1997. Energy transfer in labeled polymer chains in semidilute solutions. *Macromolecules* **10**:862–864.
36. Walter NG, Burke JM, Millar DP. 1999. Stability of hairpin ribozyme tertiary structure is governed by the interdomain junction. *Nature Struct Biol* **6**(6):544–549.

37. Walter NG, Harris DA, Pereira MJB, Rueda D. 2002. In the fluorescent spotlight: global and local conformational changes of small catalytic RNAs. *Biopolymers* **61**:224–241.
38. Yang M, Millar DP. 1997. Fluorescence resonance energy transfer as a probe of DNA structure and function. *Methods Enzymol* **278**: 417–444.
39. Eis PS, Millar DP. 1993. Conformational distributions of a four-way DNA junction revealed by time-resolved fluorescence resonance energy transfer. *Biochemistry* **32**:13852–13860.
40. Clegg RM, Murchie AIH, Lilley DM. 1994. The solution structure of the four-way DNA junction at low-salt conditions: a fluorescence resonance energy transfer analysis. *Biophys J* **66**:99–109.
41. Yang M, Millar DP. 1996. Conformational flexibility of three-way DNA junctions containing unpaired nucleotides. *Biochemistry* **35**:7959–7967.
42. Lillo MP, Szpikowska BK, Mas MT, Sutin JD, Beechem JM. 1997. Real-time measurement of multiple intramolecular distances during protein folding reactions: a multisite stopped-flow fluorescence energy-transfer study of yeast phosphoglycerate kinase. *Biochemistry* **36**: 11273–11281.
43. Lillo MP, Beechem JM, Szpikowska BK, Sherman MA, Mas MT. 1997. Design and characterization of a multisite fluorescence energy-transfer system for protein folding studies: a steady-state and time-resolved study of yeast phosphoglycerate kinase. *Biochemistry* **36**:11261–11272.
44. Ratner V, Kahana E, Eichler M, Haas E. 2002. A general strategy for site-specific double labeling of globular proteins for kinetic FRET studies. *Bioconjugate Chem* **13**:1163–1170.
45. Rice KG, Wu P, Brand L, Lee YC. 1991. Interterminal distance and flexibility of a triantennary glycopeptide as measured by resonance energy transfer. *Biochemistry* **30**:6646–6655.
46. Brown MP, Toptygin D, Lee KB, Animashaun T, Hughes RC, Lee YC, Brand L. 1998. The tryptophan fluorescence of *tetracarbidium conophorum* agglutinin II and a solution-based assay for the binding of a biantennary glycopeptide. *J Protein Chem* **17**(2):149–159.
47. Rice KG. 2001. Application of fluorescence resonance energy transfer to analyze carbohydrates. *Anal Biochem* **297**:117–122.
48. Wu P, Lee KB, Lee YC, Brand L. 1996. Solution conformations of a biantennary glycopeptide and a series of its exoglycosidase products from sequential trimming of sugar residues. *J Biol Chem* **271**(3): 1470–1474.
49. Deniz AA, Laurence TA, Beligere GS, Dahan M, Martin AB, Chemla DS, Dawson PE, Schultz PG, Weiss S. 2000. Single-molecule protein folding: diffusion fluorescence resonance energy transfer studies of the denaturation of chymotrypsin inhibitor 2. *Proc Natl Acad Sci USA* **97**:5179–5184.
50. Elangovan M, Day RN, Periasamy A. 2002. Nanosecond fluorescence resonance energy transfer-fluorescence lifetime imaging microscopy to localize the protein interactions in a single living cell. *J Microsc* **205**:3–14.
51. Wouters FS, Bastiaens PIH. 1999. Fluorescence lifetime imaging of receptor tyrosine kinase activity in cells. *Curr Biol* **9**:1127–1130.
52. Wallrabe H, Stanley M, Periasamy A, Barroso M. 2003. One- and two-photon fluorescence resonance energy transfer microscopy to establish a clustered distribution of receptor–ligand complexes in endocytic membranes. *J Biomed Opt* **8**(3):339–346.
53. Krishnan RV, Masuda A, Centonze VE, Herman B. 2003. Quantitative imaging of protein-protein interactions by multiphoton fluorescence lifetime imaging microscopy using a streak camera. *J Biomed Opt* **8**(3):362–367.
54. Mills JD, Stone JR, Rubin DG, Melon DE, Okonkwo DO, Periasamy A, Helm GA. 2003. Illuminating protein interactions in tissue using confocal and two-photon excitation fluorescent resonance energy transfer microscopy. *J Biomed Opt* **8**(3):347–356.
55. Tramier M, Gautier I, Piolot T, Ravalet S, Kemnitz K, Coppey J, Durieux C, Mignotte V, Coppey-Moisan M. 2002. Picosecond-hetero-FRET microscopy to probe protein-protein interactions in live cells. *Biophys J* **83**:3570–3577.
56. Bacskai BJ, Skoch J, Hickey GA, Allen R, Hyman BT. 2003. Fluorescence resonance energy transfer determinations using multiphoton fluorescence lifetime imaging microscopy to characterize amyloid-beta plaques. *J Biomed Opt* **8**(3):368–375.
57. Lakowicz JR, Kusba J, Wiczk W, Gryczynski I, Johnson ML. 1990. End-to-end diffusion of a flexible bichromophoric molecule observed by intramolecular energy transfer and frequency domain fluorometry. *Chem Phys Lett* **173**:319–326.
58. Lakowicz JR, Gryczynski I, Kusba J, Wiczk W, Szmacinski H, Johnson ML. 1994. Site-to-site diffusion in proteins as observed by energy transfer and frequency domain fluorometry. *Photochem Photobiol* **59**:16–29.
59. Kusba J, Lakowicz JR. 1994. Diffusion-modulated energy transfer and quenching: analysis by numerical integration of diffusion equation in Laplace space. *Methods Enzymol* **240**:216–262.
60. Lakowicz JR, Kusba J, Wiczk W, Gryczynski I, Szmacinski H, Johnson ML. 1991. Resolution of the conformational distribution and dynamics of a flexible molecule using frequency domain fluorometry. *Biophys Chem* **39**:79–84.
61. Lakowicz JR, Wiczk W, Gryczynski I, Szmacinski H, Johnson ML. 1990. Influence of end-to-end diffusion on intramolecular energy transfer as observed by frequency-domain fluorometry. *Biophys Chem* **38**:99–109.
62. Somogyi B, Matko J, Papp S, Hevessy J, Welch GR, Damjanovich S. 1984. Förster-type energy transfer as a probe for changes in local fluctuations of the protein matrix. *Biochemistry* **23**:3404–3411.
63. Haran G, Haas E, Szpikowska BK, Mas MT. 1992. Domain motions in phosphoglycerate kinase: determination of interdomain distance distributions by site-specific labeling and time-resolved fluorescence energy transfer. *Proc Natl Acad Sci USA* **89**:11764–11768.
64. Gerstein M, Lesk AM, Chothia C. 1994. Structural mechanisms for domain movements in proteins. *Biochemistry* **33**(22):6738–6749.
65. Blackwell MF, Gounaris K, Zara SJ, Barber J. 1987. A method for estimating lateral diffusion coefficients in membranes from steady state fluorescence quenching studies. *J Biophys Soc* **51**:735–744.
66. Ollmann M, Schwarzmann G, Sandhoff K, Galla H-J. 1987. Pyrene-labeled gangliosides: micelle formation in aqueous solution, lateral diffusion, and thermotropic behavior in phosphatidylcholine bilayers. *Biochemistry* **26**:5943–5952.
67. Buckler DR, Haas E, Scheraga HA. 1995. Analysis of the structure of ribonuclease A in native and partially denatured states by time-resolved nonradiative dynamic excitation energy transfer between site-specific extrinsic probes. *Biochemistry* **34**:15965–15978.

REPRESENTATIVE PUBLICATIONS ON MEASUREMENT OF DISTANCE DISTRIBUTIONS

Proteins—Distance Distributions

Amir D, Haas E. 1987. Estimation of intramolecular distance distributions in bovine pancreatic trypsin inhibitor by site-specific labeling and nonradiative excitation energy-transfer measurements. *Biochemistry* **26**:2162–2175.

Amir D, Haas E. 1988. Reduced bovine pancreatic trypsin inhibitor has a compact structure. *Biochemistry* **27**:8889–8893.

Amir D, Levy DP, Levin Y, Haas E. 1986. Selective fluorescent labeling of amino groups of bovine pancreatic trypsin inhibitor by reductive alkylation. *Biopolymers* **25**:1645–1658.

Amir D, Varshavski L, Haas E. 1985. Selective fluorescent labeling at the α–amino group of bovine pancreatic trypsin inhibitor. *Biopolymers* **24**:623-638.

Beals JM, Haas E, Krausz S, Scheraga HA. 1991. Conformational studies of a peptide corresponding to a region of the C-terminus of ribonuclease A: implications as a potential chain-folding initiation site. *Biochemistry* **30**:7680–7692.

Haas E, McWherter CA, Scheraga HA. 1988. Conformational unfolding in the N-terminal region of ribonuclease A detected by nonradiative energy transfer: distribution of interresidue distances in the native, denatured, and reduced–denatured states. *Biopolymers* **27**:1-21.

Haran G, Haas E, Szpikowska BK, Mas MT. 1992. Domain motions in phosphoglycerate kinase: determination of interdomain distance distributions by site-specific labeling and time-resolved fluorescence energy transfer. *Proc Natl Acad Sci USA* **89**:11764–11768.

DNA Structures

Clegg RM, Murchie AIH, Zechel A, Lilley DMJ. 1993. Observing the helical geometry of double-stranded DNA in solution by fluorescence resonance energy transfer. *Proc Natl Acad Sci USA* **90**:2994–2998.

McKinney SA, Déclais AC, Lilley DMJ, Ha T. 2003. Structural dynamics of individual Holliday junctions. *Nature Struct Biol* **10**(2):93–97.

Miick SM, Fee RS, Millar DP, Chazin WJ. 1997. Crossover isomer bias is the primary sequence-dependent property of immobilized Holliday junctions. *Proc Natl Acad Sci USA* **94**:9080–9084.

Mizukoshi T, Kodama TS, Fujiwara Y, Furuno T, Nakanishi M, Iwai S. 2001. Structural study of DNA duplexes containing the (6-4) photoproduct by fluorescence resonance energy transfer. *Nucleic Acids Res* **29**(24):4948–4954.

Murchie AIH, Clegg RM, von Kitzing E, Duckett DR, Diekmann S, Lilley DMJ. 1989. Fluorescence energy transfer shows that the four-way DNA junction is a right-handed cross of antiparallel molecules. *Nature* **341**:763–766.

Norman DG, Grainger RJ, Uhrín D, Lilley DMJ. 2000. Location of cyanine-3 on double-stranded DNA: importance for fluorescence resonance energy transfer studies. *Biochemistry* **39**:6317–6324.

Parkhurst KM, Parkhurst LJ. 1995. Donor–acceptor distributions in a double-labeled fluorescent oligonucleotide both as a single strand and in duplexes. *Biochemistry* **34**:293–300.

Patel LR, Curran T, Kerppola TK. 1994. Energy transfer analysis of Fos-Jun dimerization and DNA binding. *Proc Natl Acad Sci USA* **91**:7360–7364.

Ramirez-Carrozzi VR, Kerppola TK. 2001. Dynamics of Fos–Jun–NFAT1 complexes. *Proc Natl Acad Sci USA* **98**(9):4893–4898.

Tsuji A, Sato Y, Hirano M, Suga T, Koshimoto H, Taguchi T, Ohsuka S. 2001. Development of a time-resolved fluorometric method for observing hybridization in living cells using fluorescence resonance energy transfer. *Biophys J* **81**:501–515.

End-to-End Diffusion

Bandyopadhyay T, Ghosh SK. 2003. Diffusion assisted end-to-end relaxation of a flexible Rouse polymer chain: fluorescence quenching through a model energy transfer. *J Chem Phys* **119**(1):572–584.

Duus JØ, Meldal M, Winkler JR. 1998. Fluorescence energy-transfer probes of conformation in peptides: the 2-aminobenzamide/nitrotyrosine pair. *J Phys Chem B* **102**:6413–6418.

Gryczynski I, Lakowicz JR, Kusba J. 1995. End-to-end diffusion coefficients and distance distributions from fluorescence energy transfer measurements: enhanced resolution by using multiple donors with different lifetimes. *J Fluoresc* **5**(2):195–203.

Lakowicz JR, Kusba J, Gryczynski I, Wiczk W, Szmacinski H, Johnson M. 1991. End-to-end diffusion and distance distributions of flexible donor–acceptor systems observed by intramolecular energy transfer and frequency-domain fluorometry; enhanced resolution by global analysis of externally quenched and nonquenched samples. *J Phys Chem* **95**:9654–9660.

Lakowicz JR, Nair R, Piszczek G, Gryczynski I. 2000. End-to-end diffusion on the microsecond timescale measured with resonance energy transfer from a long-lifetime rhenium metal–ligand complex. *Photochem Photobiol* **71**(2):157–161.

Maliwal BP, Lakowicz JR. 1993. Fluorescence study of conformational flexibility of RNAse S-peptide: distance-distribution, end-to-end diffusion and anisotropy decays. *Biochemistry* **32**:12337–12345.

Maliwal BP, Kusba J, Wiczk W, Johnson M, Lakowicz JR. 1993. End-to-end diffusion coefficients and distance distributions from fluorescence energy transfer measurements: enhanced resolution by using multiple acceptors with different Förster distances. *Biophys Chem* **46**:273–281.

Neuweiler H, Schulz A, Böhmer M, Enderlein J, Sauer M. 2003. Measurement of submicrosecond intramolecular contact formation in peptides at the single-molecule level. *J Am Chem Soc* **125**:5324–5330.

Nyitrai M, Hild G, Bódis E, Lukács A, Somogyi B. 2000. Flexibility of myosin-subfragment-1 in its complex with actin as revealed by fluorescence resonance energy transfer. *Eur J Biochem* **267**:4334–4338.

Talaga DS, Lau WL, Roder H, Tang J, Jia Y, DeGrado WF, Hochstrasser RM. 2000. Dynamics and folding of single two-stranded coiled-coil peptides studied by fluorescent energy transfer confocal microscopy. *Proc Natl Acad Sci USA* **97**(24):13021–13026.

Reviews

Wemmer DA, Case DA, Millar DP. 2002. Fluorescence spectroscopy and nucleic acids. *Biopolymers Nucleic Acid Sci* **61**(3):143–242.

Ribozymes

Lafontaine DA, Norman DG, Lilley DMJ. 2002. The global structure of the VS ribozyme. *EMBO J* **21**(10):2461–3471.

Tan E, Wilson TJ, Nahas MK, Clegg RM, Lilley DMJ, Ha T. 2003. A four-way junction accelerates hairpin ribozyme folding via a discrete intermediate. *Proc Natl Acad Sci USA* **100**(16):9308–9313.

Walter F, Murchie AIH, Duckett DR, Lilley DMJ. 1998. Global structure of four-way RNA junctions studied using fluorescence resonance energy transfer. *RNA* **4**:719–728.

Walter F, Murchie AIH, Thomson JB, Lilley DMJ. 1998. Structure and activity of the hairpin ribozyme in its natural junction conformation: effect of metal ions. *Biochemistry* **37**:14195–14203.

Wilson TJ, Lilley DMJ. 2002. Metal ion binding and the folding of the hairpin ribozyme. *RNA* **8**:587–600.

Ribozomes

Klostermeier D, Sears P, Wong CH, Millar DP, Williamson JR. 2004. A three-fluorophore FRET assay for high-throughput screening of small-molecule inhibitors of ribosome assembly. *Nucleic Acids Res* **32**(9):2707–2715.

Melcher SE, Wilson TJ, Lilley DMJ. 2003. The dynamic nature of the four-way junction of the hepatitis C virus IRES. *RNA* **9**:809–820.

Theory

Farinha JPS, Spiro JG, Winnik MA. 2004. Dipole–dipole electronic energy transfer: fluorescence decay functions for arbitrary distributions of donors and acceptors in systems with cylindrical symmetry. *J Phys Chem B* **108**:16392–16400.

Rolinski O, Birch DJS, McCartney LJ, Pickup JC. 2000. A method of determining donor acceptor distribution functions in Förster resonance energy transfer. *Chem Phys Lett* **324**:95–100.

Rolinski O, Birch DJS, McCartney LJ, Pickup JC. 2001. Fluorescence nanotomography using resonance energy transfer: demonstration with a protein–sugar complex. *Phys Med Biol* **46**:N221–N226.

Srinivas G, Yethiraj A, Bagchi B. 2001. FRET by FET and dynamics of polymer folding, 2001. *J Phys Chem* **105**(13):2475–2478.

Valeur B, Mugnier J, Pouget J, Bourson J, Santi F. 1989. Calculation of the distribution of donor–acceptor distances in flexible bichromophoric molecules: application to intramolecular transfer of excitation energy. *J Phys Chem* **93**:6073–6079.

PROBLEMS

Intensity Decays for Various Donor–Acceptor Pairs: Assume that you have three different solutions. All contain donors that display the same quantum yield, a single-exponential decay time of 5 ns in the absence of acceptor, and the same Förster distance of 20 Å. One sample (A) consists of a protein with a single donor and three acceptors at distances r_1 = 15 Å, r_2 = 20 Å, and r_3 = 25 Å (Figure 14.34). The second sample (B) contains three equimolar proteins, each with a single donor and acceptor. However, in each protein there is a different D–A distance: 15, 20, or 25 Å. The third sample (C) is a protein with a single acceptor, but with three donors. Each donor displays the same donor-alone lifetime (τ_D = 5 ns), but a different distance (15, 20, or 25 Å) from the acceptor.

P14.1. Describe the intensity decays of samples A, B, and C. Which samples display a single- or multi-exponential decay law?

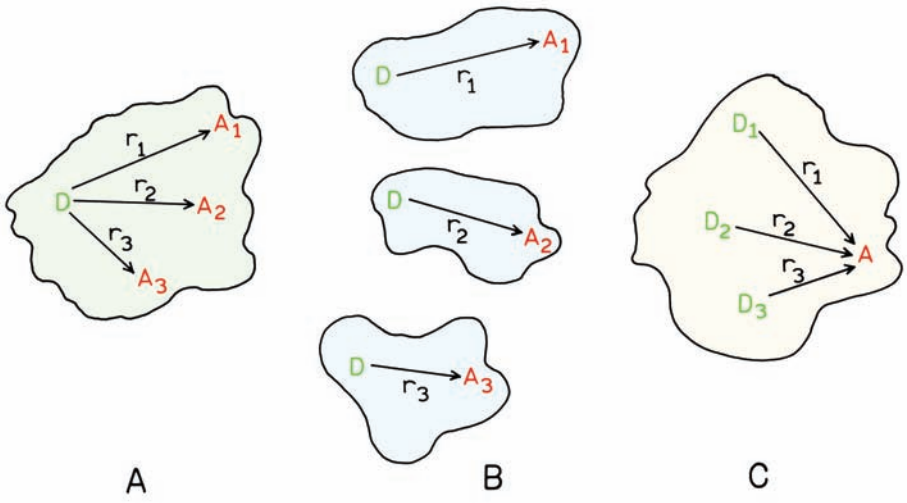

Figure 14.34. Schematic of a protein with three acceptors (A), three proteins each with a single acceptor (B), and a protein with three donors and one acceptor (C). The distances are r_1 = 15 Å, r_2 = 20 Å, and r_3 = 25 Å. The Förster distance is 20 Å. See Problem 14.1.

P14.2. Describe the intensity decay law of sample B, including the decay times, pre-exponential factors (α_i) and fractional intensity (f_i) values. Assume each protein is present in equimolar amounts.

P14.3. For the three-acceptor protein (sample A), could you detect the presence of three acceptors from the intensity decay?

P14.4. For the three-acceptor protein what is the apparent D–A distance if you assumed the presence of a single acceptor?

P14.5. *Acceptor Concentration for FRET for Unlinked D–A Pairs*:

(a) Suppose you have a donor and acceptor that are not covalently linked, and that the Förster distance is 30 Å. Calculate the acceptor concentration needed to place, on average, one acceptor within a 60-Å cube containing a donor at the center. To a first approximation this concentration is comparable to that for 50% energy transfer. Compare this acceptor concentration with that calculated using eq. 13.33.

(b) Consider a D–A pair covalently linked by a 30-Å linker. Calculate the effective concentration of acceptors around the donor.